Contributions to Mineralogy and Petrology (2023) 178:38
https://doi.org/10.1007/s00410-023-02013-z

ORIGINAL PAPER

Progressive carbonation and Ca-metasomatism of serpentinized ultramafic rocks: insights from natural occurrences and hydrothermal experiments

Nomuulin Amarbayar[1,2] · Otgonbayar Dandar[1,2] · Jiajie Wang[1] · Atsushi Okamoto[1] · Masaoki Uno[1] · Undarmaa Batsaikhan[2,3] · Hideko Takayanagi[4] · Yasufumi Iryu[4] · Noriyoshi Tsuchiya[1]

Received: 6 July 2022 / Accepted: 13 April 2023 / Published online: 16 June 2023

Abstract

Hydration, carbonation, and related metasomatism of mantle peridotite play a significant role in the global geochemical cycle. In this study, we combined an analysis of carbonated serpentinite with hydrothermal experiments on carbonation and Ca-metasomatism for samples from the Manlay ophiolite, southern Mongolia to investigate that carbonation mechanism of the serpentinite body after serpentinization. Samples show that the serpentinite was either transected by calcite and dolomite veins or was completely replaced by carbonates (calcite with minor dolomite) and quartz, in which the original mesh texture of serpentinite was preserved. Carbonation occurred after low-temperature serpentinization (lizardite/chrysotile), suggesting that carbonation occurred at temperatures lower than 300 ˚C. Calcite in the serpentinite showed $\delta^{13}C_{VPDB}$ values ranging from -8.83 to -5.11 ‰ and $\delta^{18}O_{VSMOW}$ from + 20.1 to + 24.4 ‰, suggesting that CO_2 in the fluids could be derived from the degradation of organic material or methanotrophic processes rather than the origin of seafloor limestone. Three batch-type experiments, i.e., single step experiments (1) Olivine + $NaHCO_{3,aq}$ + $CaCl_{2,aq}$ and (2) Chrysotile + $NaHCO_{3,aq}$ + wollastonite (Ca source), and two steps experiment (3) Olivine carbonation and Ca-metasomatism, were conducted at 275 °C and 5.7 MPa to constrain the mechanism of calcite replacement of serpentinite. We found that calcite precipitated from the solution directly in the first two experiments, but replacement of serpentinite by calcite was not observed. In contrast, the third experiment caused the initial carbonation to form magnesite and then changed to calcite by later alteration. The natural occurrences and experiments revealed the possibility that the carbonation of olivine followed by Ca-rich fluid infiltration produced calcite in the carbonated serpentinite. Such Ca-metasomatism of Mg carbonates could easily occur in the ultramafic bodies and significantly affect the global carbon cycle.

Keywords Replacement · Manlay ophiolite · Carbonation · Ca-metasomatism · Carbon storage

Introduction

Carbonation is a crucial alteration process that converts silicate and hydroxide minerals into carbonate minerals such as calcite, aragonite, dolomite, magnesite, and siderite, with implications from the global carbon cycle, formation of ore deposits, and CO_2 sequestration (Phillips and Evans 2004; Kelemen and Matter 2008; Bjerga et al. 2015; Boskabadi et al. 2020; Oyanagi et al. 2021). The presence of silicate minerals, such as olivine and pyroxene, in mantle peridotite and basalt make them highly susceptible to carbonation reactions (Kelemen et al. 2011; Boskabadi et al. 2020) such as olivine reacting with a CO_2-rich fluid to form magnesite (Eq. 1). In the $MgO–SiO_2–H_2O–CO_2$ system, typical

Communicated by Timm John.

✉ Noriyoshi Tsuchiya
noriyoshi.tsuchiya.a1@tohoku.ac.jp

1 Graduate School of Environmental Studies, Tohoku University, Aoba 6-6-20, Aramaki Aoba-ku, Sendai 980-8579, Japan

2 Geoscience Center, School of Geology and Mining, Mongolian University of Science and Technology, Ulaanbaatar 14191, Mongolia

3 School of Geology and Mining, Mongolian University of Science and Technology, Ulaanbaatar 14191, Mongolia

4 Graduate School of Science, Tohoku University, Aobayama, Sendai 980-8578, Japan

carbonation reactions after olivine is written as follows (e.g., Grozeva et al. 2017);

$$Mg_2SiO_4\,(\text{Olivine}) + 2CO_2 = 2MgCO_3\,(\text{Magnesite}) + SiO_2,\,(\text{Quartz}) \quad (1)$$

The magnesite + quartz assemblage (known as listvenite) is commonly found in carbonated ultramafic rocks from numerous ophiolite complexes (e.g., Ulrich et al. 2014; Falk and Kelemen 2015; Menzel et al. 2018, 2022; Boskabadi et al. 2020). A similar reaction pathway is preserved in the carbonation of serpentinized ultramafic rock and serpentinite (Eq. 2; Kelemen and Hirth 2012; Menzel et al. 2022) as follows:

$$Mg_3Si_2O_5\,(OH)_4\,(\text{Serpentine}) + 3CO_2 = 3MgCO_3\,(\text{Magnesite}) + 2SiO_2\,(\text{Quartz}) + 2H_2O. \quad (2)$$

The fluid composition corresponding to carbonation reactions (Eq. 1 and Eq. 2) can be predicted by thermodynamic models (Klein and Garrido 2011).

The formation of magnesite (Eqs. 1 and 2) can easily occur by reacting Mg^{2+} ion liberated from the Mg-bearing minerals in ultramafic rocks with external CO_2 fluids. Ca-carbonate (calcite) and Ca-Mg carbonate (dolomite) are also often observed in association with serpentinites. In these cases, as Ca is not always abundant in the serpentinites, Ca should be transported from the external sites as well as CO_2 to form Ca-carbonates. Therefore, calcite and dolomite commonly occur in fractures and vugs within the ultramafic rocks (e.g. Falk et al. 2016; Hinsken et al. 2017; Lafay et al. 2017; Boskabadi et al. 2020; Okamoto et al. 2021). For example, the fully carbonated ultramafic body of the Oman ophiolite shows the cross-cutting relationship between carbonate minerals, with coarse dolomite and calcite veines cutting fine-grained magnesite-quartz listvenite (e.g., Falk and Kelemen 2015). In the Wadi Fins of the Oman ophiolite, the polygonal vein networks composed of serpentine + calcite were developed in the serpentinized peridotite body overlain by oceanic limestone (de Obeso and Kelemen 2018).

Calcite, magnesite, and dolomite demonstrate the varying stability fields at elevated temperatures and pressures (e.g., Kerrick and Connelly 2001). Therefore, when they enter the Earth's interior, the type of carbonate minerals (Ca-carbonates vs. Mg carbonates) formed into the ultramafic body during CO_2 uptake near surface conditions could provide significant influences on the global carbon cycle (Galvez and Pubellier 2019). However, due to the complex vein structures composed of various carbonates in the carbonated serpentinites, the mechanism of carbonation related to fracturing and mass transport including Ca, Mg, and silica is not yet fully understood.

In this study, we investigate the mineralogy and microstructures of carbonated serpentinite bodies of the Manlay ophiolite in Mongolia. We present a unique example of pervasive serpentinite carbonation, where the serpentinite was replaced by calcite + quartz assemblage, but it preserves mesh textures of the original serpentinite. In this case, Mg in the serpentinites should be removed from the body. In order to understand the mechanism of the replacement of serpentinite by Ca-carbonate, we conducted three hydrothermal experiments (single step: Olivine + $NaHCO_{3,aq}$ + $CaCl_{2,aq}$ and Chrysotile + $NaHCO_{3,aq}$ + wollastonite, and two steps: Olivine carbonation and Ca-metasomatism). Combining natural occurrences and the results of the hydrothermal experiments, we discuss the relationship between serpentinization, carbonation and Ca-metasomatism of the ultramafic body.

Geological background: natural partially and completely carbonated serpentinites from the Manlay ophiolite

The Manlay ophiolite complex, one of the largest and most well-preserved ophiolite in southern Mongolia is made up predominantly of ultramafic rocks, basalts, and cherts (Zhu et al. 2014). The Manlay ophiolite of the Cambrian age has a supra-subduction signature and is thought to be the basement of late Paleozoic arc formations in southern Mongolia (Fig. 1a and b; Zhu et al. 2014). Basalt with minor chert, ultramafic rock, plagiogranite, gabbro, and pyroxenite occur in the western part, while the eastern part is dominated by secondary carbonated ultramafic rocks, and dolerite intrusion, thin chromitite veins. In contrast, andesite and tuffaceous sandstone interlayered with siliceous shale occur in the northwestern part along with pillow lavas in the southeastern part.

The plagiogranite and gabbro exposed in the western part have yielded U–Pb ages of 482–509 Ma (Zhu et al. 2014). Whole-rock geochemical data of igneous rocks suggests that the origin of the Manlay ophiolite is a supra-subduction zone, as large-ion lithophile elements (LILE) and light rare earth elements (LREE) are enriched in basalt and dolerite samples with negative Nb, Ta, Ti, and weak Eu anomalies (Zhu et al. 2014). In addition, ultramafic rocks occur as small elongated bodies (approximately 1 km thick) and have very high loss of ignition values that correspond to extensive serpentinization and carbonation (Zhu et al. 2014). The chemistry of spinel in ultramafic rocks of the Manlay ophiolite supports that it was formed in the supra-subduction zone (Amarbayar et al. 2021; Zhu et al. 2014).

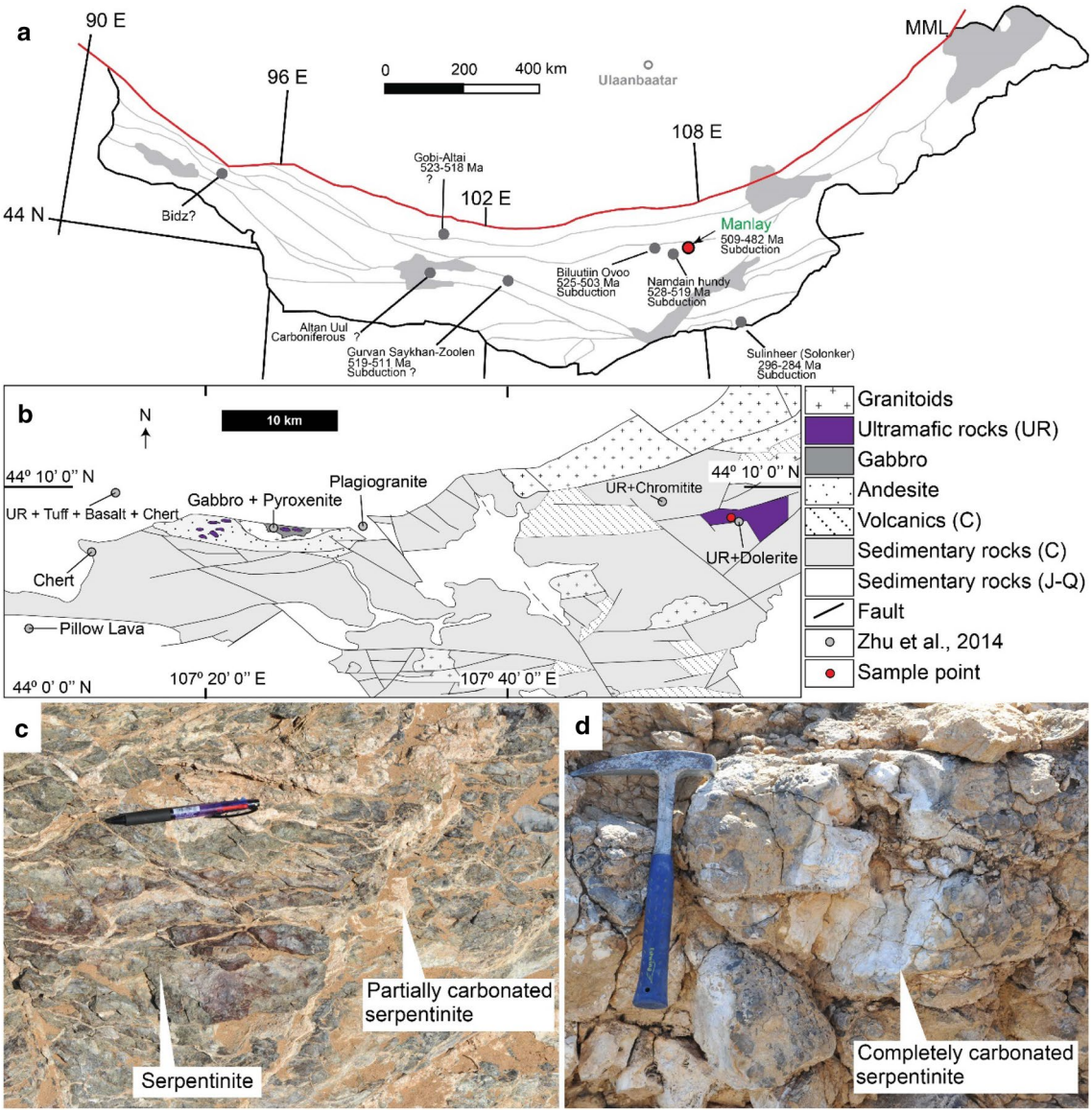

Fig. 1 Location of the Manlay Ophiolite. **a** Simplified terrane map of southern Mongolia and ophiolite distribution in southern Mongolia (modified from Badarch et al. 2002; Furnes and Safonova 2019). Ophiolites are shown with ages and tectonic settings. Question marks indicate uncertain ages or tectonic settings. The gray open circle indicates the location of the city of Ulaanbaatar. Gray circles indicate localities of ophiolite in southern Mongolia. The red circle shows the location of the Manlay Ophiolite. The red line is the Main Mongolian Lineament (MML). C, J, and Q indicate Carboniferous, Jurassic, and Quaternary, respectively. UR indicates ultramafic rock. **b** Simplified geological map of the eastern side of the Manlay Ophiolite (modified from Zhu et al. (2014)). **c** Field photo of partially carbonated serpentinite in the Manlay Ophiolite. **d** Field photo of completely carbonated serpentinite in the Manlay Ophiolite

Recently, Amarbayar et al. (2021) investigated the ultramafic body within the Manlay ophiolite and presented its three-stage serpentinization history as: (1) replacement of olivine by lizardite, (2) chrysotile formation (bastite) after orthopyroxene and as a replacement of olivine relics; and (3) development of chrysotile veins that crosscut all previous textures. They referred to the carbonation occurring in this serpentinite body (Fig. 1 c and d). However, petrological and mineralogical characteristics of the carbonated serpentinite has not been described in detail, whilst the mechanism of how carbon dioxide was stored in hydrated ultramafic rock remains unclear.

Methods

Analyses of the naturally carbonated serpentinites

The mineralogy and microstructures of the carbonated serpentinites from the Manlay ophiolite were observed in thin

sections using an optical microscope. The mineral assemblages of the collected samples are listed in Table 1. Serpentine and carbonate minerals were identified using a Raman spectrometer (Horiba XploRa) equipped with an Olympus BX51 microscope at Tohoku University whose calibration was performed using synthetic silicon and the 520 cm^{-1} band. The estimated spectral resolution was 1.0 cm^{-1}; the grating, objective, and laser spot sizes were 1800 g/mm, × 100, and 1 μm, respectively. A green laser was used with a wavelength and integration time of 532 nm and 5 s, respectively. The carbonate phases were identified by referring to Edwards et al. (2005). The Raman spectra of the quartz, calcite, and dolomite are shown in Fig. S1.

The chemical compositions of the minerals were determined using an electron probe microanalyzer (EPMA; JEOL JXA-8200) at Tohoku University. The natural and synthetic standards used for the calibration were wollastonite for Ca and Si, rutile for Ti, eskolaite for Cr, hematite for Fe, corundum for Al, manganosite for Mn, periclase for Mg, albite for Na, and feldspar for K. The accelerating voltage and beam currents were set at 15 kV and 12 nA for quantitative analyses and 15 kV and 120 nA for mapping. The focused beam diameter was 1–5 μm. The representative chemical composition of the minerals is presented in Table 2.

A micro-sampling technique using a hand-held needle drill was utilized to analyze the carbon and oxygen stable isotopes. Contamination was avoided by sampling each target spot after mechanical abrasion of the surface. Sample powders (~ 0.1 mg) were reacted with 100% phosphoric acid at ~ 72 °C. The isotope compositions were measured using a Thermo Fisher (Waltham, MA) Delta V isotope ratio mass spectrometer equipped with a ThermoQuest (Bremen, Germany) Kiel-III automated carbonate device at Tohoku University. Although some samples contained silicate minerals (serpentine and quartz), they were almost insoluble in phosphoric acid at 72 °C. Although some samples included small amounts of dolomite veins, dolomite dissolution is more sluggish than calcite dissolution in phosphoric acid within a short period (approximately 25 min) at 72 °C (e.g. Okamoto et al. 2021), and is negligible. Therefore, the effect of silicate minerals and dolomite on isotope compositions is negligible. The isotope ratios were expressed in conventional (δ ‰) notation and calibrated using the NBS-19 international standard relative to the Veinna Pee Dee Belemnite (VPDB). The external precision (1σ) for the carbon and oxygen isotope analyses based on replicate measurements of the laboratory reference materials JCp-1 was 0.03 and 0.03‰, respectively. δ^{18} O [‰ VPDB] was converted to δ^{18} O [‰ VSMOW] using Coplen et al.'s (1983) equation. Carbon and oxygen isotope compositions are listed in Table 3 and the analysis spots are shown in Supplementary Fig. S2.

Hydrothermal experiments

Three hydrothermal experiments on olivine hydration and carbonation were designed to address the formation of calcium carbonates in ultramafic rocks of the Manlay ophiolite (the experimental conditions are summarized in Table 4).

Powders of olivine (Damaping, China), chrysotile (Khantaishir Ophiolite; Mongolia; Dandar et al. 2019), and wollastonite (Aichi, Japan) were used as the starting materials. Olivine and wollastonite were natural pure minerals, with Mg# (= $Mg/(Mg + Fe^{2+})$) of 0.92 and Ca# (= $Ca/(Mg + Ca + Fe^{2+})$) of 0.99, respectively. Chrysotile samples from the Khantaishir ophiolite contain a small amount of calcite and magnetite. Thus the sample was digested in 1 mol/L HCl for 24 h to dissolve the calcite, followed by filtration and washing of the digested sample using Milli-Q water. The residual magnetite was removed with a magnetic stirrer in an aqueous phase. All minerals were crushed and sieved to a size < 100 μm. $NaHCO_3$ (Kanto Chemical, Japan) and $CaCl_2$ (Fujifilm Wako Chemical, Japan), with purities > 99.0%, were utilized to make CO_2 and Ca-rich water solutions.

A batch-type autoclave made of Hastelloy-C, with an internal volume of 170 mL, was used for the hydrothermal experiments (Fig. 2). All experiments were performed at 275 °C and 5.7 MPa (vapor-saturated pressure), according to Wang et al. (2019).

The results of the first run are presented in Table 4 (no. Ol_NaCa), a single-step experiment in a system of olivine + $NaHCO_{3,\,aq}$ + $CaCl_{2,\,aq}$ + H_2O, which simulated the

Table 1 The mineral assemblage of the partially and completely carbonated ultramafic rock samples from the Manlay ophiolite

Sample no	Lithology	Primary			Secondary				
		Ol/Opx	Spl	Cpx	Ser	Mgt	Cal	Dol	Qz
18091302Ca01	Partially carbonated serpentinite		+	+	+	+	+	+	
18091302Ca02	Partially carbonated serpentinite		+	+	+	+	+	+	
18091302Ca03	Partially carbonated serpentinite		+	+	+	+	+		
18091302Ca04	Partially carbonated serpentinite		+		+	+	+	+	
18091302Ca05	Partially carbonated serpentinite		+		+	+	+	+	
1,809,130,211	Completely carbonated serpentinite		+			+	+	+	+
1,809,130,204	Completely carbonated serpentinite		+		+	+	+	+	

Table 2 Representative electron microprobe data (in wt%) and calculated structural formulae (in a.p.f.u) for serpentine, spinel, magnetite, calcite, dolomite, and quartz in the partially and completely carbonated serpentinites

Lithology	Partially carbonated serpentinite					Completely carbonated serpentinite				
Mineral	Srp avg	Cal avg	Dol avg	Mgt avg	Spl avg	Cal avg	Dol avg	Mgt avg	Spl avg	Qz avg
N	1	1	1	1	1	1	1	1	1	1
SiO_2	43.69	n.d	n.d	0.41	n.d	n.d	n.d	0.04	0.05	96.95
TiO_2	n.d	n.d	0.01	0.02	0.02	n.d	0.02	< 0.01	0.15	< 0.01
Al_2O_3	1.20	0.06	0.08	< 0.01	22.37	n.d	0.06	< 0.01	7.94	< 0.01
Cr_2O_3	0.36	n.d	n.d	< 0.01	45.62	n.d	n.d	< 0.01	56.73	< 0.01
FeO	4.72	0.14	0.06	91.71	20.50	0.10	0.07	91.20	27.93	0.33
MgO	36.73	0.42	19.90	0.03	10.92	0.04	20.39	0.02	6.69	< 0.01
MnO	0.18	< 0.01	0.41	0.15	0.32	< 0.01	< 0.01	0.08	0.57	< 0.01
CaO	0.13	55.26	30.66	0.05	n.d	51.26	33.29	0.01	< 0.01	0.06
NiO	0.12	n.d	n.d	0.02	0.06	n.d	n.d	0.02	0.08	0.03
Na_2O	0.02	0.07	n.d	0.15	0.11	0.08	n.d	0.13	n.d	0.03
K_2O	n.d	n.d	n.d	< 0.01	n.d	0.01	n.d	< 0.01	n.d	< 0.01
Total	87.15	55.95	51.12	92.50	99.92	51.49	53.83	91.50	100.14	97.40
Ox	7	1	1	4	4	1	1	4	4	–
Si	2.05	n.d	n.d	0.015	n.d	n.d	n.d	< 0.01	< 0.01	–
Ti	n.d	n.d	< 0.01	< 0.01	< 0.01	n.d	< 0.01	0.010	< 0.01	–
Al	0.07	< 0.01	< 0.01	< 0.01	0.820	n.d	< 0.01	< 0.01	0.318	–
Cr	0.01	n.d	n.d	< 0.01	1.122	n.d	n.d	< 0.01	1.525	–
Fe^{3+}	–	–	–	1.978	0.063	–	–	2.008	0.146	–
Fe^{2+}	0.19	< 0.01	< 0.01	0.985	0.470	< 0.01	< 0.01	0.975	0.648	–
Mg	2.57	0.01	0.470	< 0.01	0.507	< 0.01	0.459	< 0.01	0.339	–
Mn	< 0.01	< 0.01	0.01	< 0.01	< 0.01	< 0.01	< 0.01	< 0.01	0.016	–
Ca	< 0.01	0.985	0.521	< 0.01	< 0.01	0.996	0.538	< 0.01	< 0.01	–
Ni	< 0.01	n.d	n.d	< 0.01	< 0.01	n.d	n.d	< 0.01	< 0.01	–
Na	< 0.01	< 0.01	n.d	0.011	< 0.01	< 0.01	n.d	0.010	n.d	–
K	n.d	n.d	n.d	< 0.01	n.d	< 0.01	n.d	< 0.01	n.d	–
Mg#	0.932	0.989	0.475	–	0.518	0.999	0.460	–	0.344	
Cr#					0.578				0.827	

Lithology	Partially carbonated serpentinite					Completely carbonated serpentinite				
Mineral	Srp	Cal	Dol	Mgt	Spl	Cal	Dol	Mgt	Spl	Qz
SiO_2	43.69	n.d	n.d	0.41	n.d	n.d	n.d	0.04	0.05	96.95
TiO_2	n.d	n.d	0.01	0.02	0.02	0.07	n.d	< 0.01	0.15	< 0.01
Al_2O_3	1.20	0.06	0.08	< 0.01	22.37	0.04	n.d	< 0.01	7.94	< 0.01
Cr_2O_3	0.36	n.d	n.d	< 0.01	45.62	n.d	n.d	< 0.01	56.73	< 0.01
FeO	4.72	0.14	0.06	91.71	20.50	n.d	n.d	91.20	27.93	0.33
MgO	36.73	0.42	19.90	0.03	10.92	0.97	22.00	0.02	6.69	< 0.01
MnO	0.18	< 0.01	0.41	0.15	0.32	0.08	0.08	0.08	0.57	< 0.01
CaO	0.13	55.26	30.66	0.05	n.d	56.48	29.94	0.01	< 0.01	0.06
NiO	0.12	n.d	n.d	0.02	0.06	n.d	n.d	0.02	0.08	0.03
Na_2O	0.02	0.07	n.d	0.15	0.11	n.d	n.d	0.13	n.d	0.03
K_2O	n.d	n.d	n.d	< 0.01	n.d	n.d	n.d	< 0.01	n.d	< 0.01
Total	87.15	55.95	51.12	92.50	99.92	57.64	52.03	91.50	100.14	97.40
Ox	7	1	1	4	4	1	1	4	4	–
Si	2.05	n.d	n.d	0.015	n.d	n.d	n.d	< 0.01	< 0.01	–
Ti	n.d	n.d	< 0.01	< 0.01	< 0.01	< 0.01	n.d	0.010	< 0.01	–
Al	0.07	< 0.01	< 0.01	< 0.01	0.820	< 0.01	n.d	< 0.01	0.318	–

Table 2 (continued)

Lithology	Partially carbonated serpentinite					Completely carbonated serpentinite				
Mineral	Srp	Cal	Dol	Mgt	Spl	Cal	Dol	Mgt	Spl	Qz
Cr	0.01	n.d	n.d	< 0.01	1.122	n.d	n.d	< 0.01	1.525	–
Fe^{3+}	–	–	–	1.978	0.063	–	–	2.008	0.146	–
Fe^{2+}	0.19	< 0.01	< 0.01	0.985	0.470	n.d	n.d	0.975	0.648	–
Mg	2.57	0.01	0.470	< 0.01	0.507	0.02	0.50	< 0.01	0.339	–
Mn	< 0.01	< 0.01	0.01	< 0.01	< 0.01	< 0.01	< 0.01	< 0.01	0.016	–
Ca	< 0.01	0.985	0.521	< 0.01	< 0.01	0.97	0.49	< 0.01	< 0.01	–
Ni	< 0.01	n.d	n.d	< 0.01	< 0.01	n.d	n.d	< 0.01	< 0.01	–
Na	< 0.01	< 0.01	n.d	0.011	< 0.01	n.d	n.d	0.010	n.d	–
K	n.d	n.d	n.d	< 0.01	n.d	n.d	n.d	< 0.01	n.d	–
Mg#	0.932	0.015	0.475	–	0.518	0.023	0.506	–	0.344	
Cr#					0.578				0.827	

FeO	Cr2O3	MnO	Total
0.33	0.00	0.01	97.40

Srp serpentine, *Cal* calcite, *Dol* dolomite, *Mgt* magnetite, *Spl* spinel, *Qz* quartz; n.d = not detected, (–) not calculated; mix for serpentine indicates mixture of serpentine and magnesite due to fine grain; mix for magnetite indicates mixture of magnetite and serpentine due to fine grain

Table 3 Carbon and oxygen isotopic composition of the partially and completely carbonated serpentinites from the Manlay ophiolite

Sample no	Lithology	Point	$\delta^{13}C_{VPDB}$ (‰)	$\delta^{18}O_{SMOW}$ (‰)
18091302Ca01	Partially carbonated serpentinite	Ca01_1	– 7.54	22.826
		Ca01_2	– 7.85	22.931
		Ca01_3	– 7.92	23.037
		Ca01_4	– 7.05	23.017
		Ca01_5	– 6.16	23.588
		Ca01_6	– 7.86	22.735
		Ca01_7	– 6.97	22.944
1,809,130,211	Completely carbonated serpentinite	211_1	– 5.11	22.789
		211_2	– 6.19	22.079
		211_3	– 5.15	22.821
		211_7	1.97	25.336
1809130204	Completely carbonated serpentinite	04_1	– 8.76	20.308
		04_2	– 8.83	20.056
		04_3	– 8.36	22.721
		04_4	– 8.33	22.783
		04_5	– 8.27	22.678
		04_6	– 8.73	24.393

situation where olivine was directly carbonated in a CO_2 and Ca-rich system. Five grams of olivine powder was mixed with a 100 mL solution containing 0.5 mol/L $NaHCO_3$ and 0.7 mol/L $CaCl_2$. The reaction duration was 48 h.

The second run (no. Serp_NaWo) is also a single-step experiment in which chrysotile, as a hydrated olivine sample, was used to check how it can participate in the carbonation reaction. In this study, wollastonite was used as the Ca source, as Ca-bearing clinopyroxenes could contribute to calcium carbonation (e.g., Daval et al. 2013; Kelemen et al. 2018). To create an Mg/Ca atomic ratio of 1, 5 g serpentine and 6.4 g wollastonite powders were added to 100 mL of a 0.5 mol/L $NaHCO_3$ solution for the experiment. The duration was extended to 90 h to ensure a sufficient time for wollastonite dissolution and Ca release.

The third run (no. Ol_Carb_Ca) was a two-step experiment (Table 4) that simulated the situation where olivine was first carbonated without a Ca source. After this, a Ca source was added to verify if Ca-metasomatism occurred. The first reaction step (no. Ol_Carb_step1) is olivine hydration and

Table 4 Summary of fluid chemistry for experiment 1

Experimental type	Single step experiment	Single step experiment	Two step experiment	
Run name	Ol_NaCa	Srp_NaW	Ol_Carb_Ca	
Step			Step 1	Step 2
$NaHCO_3$ (mol/L)	0.5	0.5	0.5	–
$CaCl_2$ (mol/L)	0.7	–	–	0.7
Reaction	$Ol + NaHCO_3 + CaCl_2 + H_2O$	$Srp + NaHCO_3 + Wol + H_2O$	$Ol + NaHCO_3 + H_2O$	$Ol + Srp + Mgs + CaCl_2 + H_2O$
T (°C)	275	275	275	275
Time (h)	48	90	48	56
pH				
Initial	5.0	8.2	8.2	9.4
Final	6.6	9.1	8.8	7.4
Fluid chemistry after reactions (ppm)				
Mg	–	–	2	195.1
Si	–	–	4.8	0.6
K	–	–	8.2	1.2
Ca	–	–	0.97	6226.3
Mn	–	–	0.01	1.6

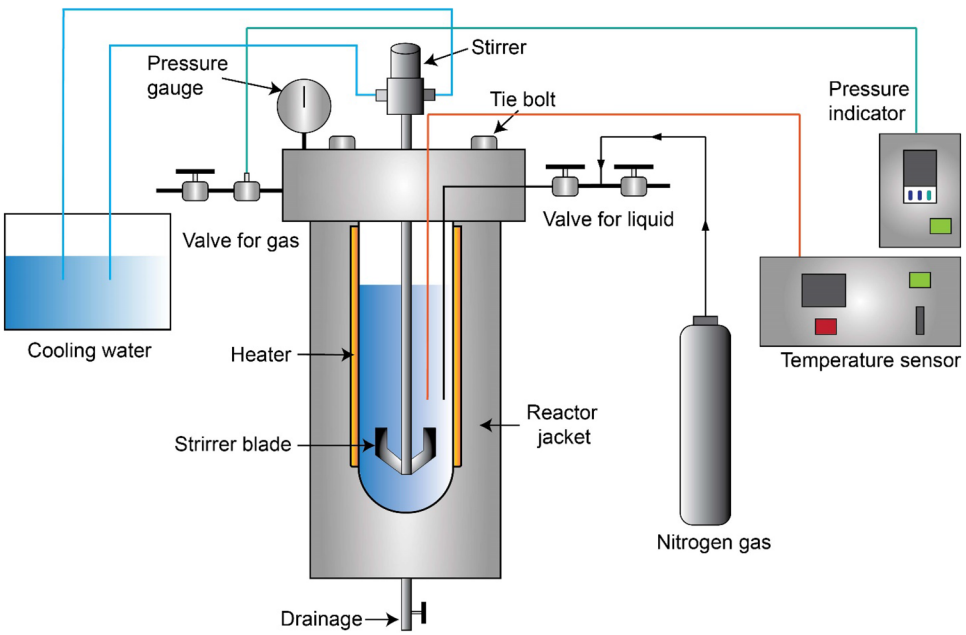

Fig. 2 Schematic diagram of the autoclave reactor (modified from the Wang et al. 2019)

carbonation of olivine in 0.5 mol/L $NaHCO_3$ solution for 48 h. After that, we removed the fluid that contained residual $NaHCO_3$ by filtration using a 0.45 µm membrane and washed the solid sample with Milli-Q water several times. The second step (no. Ol_Ca_step2) was Ca replacement of the Mg-bearing mineral products in the first step with Ca-rich fluid. Here, a 0.7 mol/L $CaCl_2$ solution was used as a Ca-rich fluid. The duration was 56 h.

In all experiments, the solution volume was 100 mL, and the water/rock mass ratio was 20. After enclosing the mineral powders and solutions, the reactor was closed and flushed with N_2 gas for 10 min to eliminate any dissolved O_2. Subsequently, the internal temperature and pressure were increased to the desired values and were maintained for 48–90 h for hydrothermal reactions. After each reaction, the reactor was cooled to below 50 °C in 5 min by circulating cold water, and the reaction was stopped.

Analyses of the experimental products

After each experimental step, the solid and liquid samples were separated by filtration using a 0.45 µm membrane. Solid samples were washed with Milli-Q water and dried at 50 °C for 24 h in an oven for further analysis.

The mineral assemblage of the solid products was investigated by X-ray diffraction (XRD; MiniFlex, Rigaku, Japan) with Cu Kα radiation operated at 40 kV and 15 mA with a 2θ step size of 0.02°. The initial and newly generated mineral morphologies were examined using scanning electron microscopy (SEM, SU-8000, Hitachi) equipped with energy dispersive spectroscopy (EDS). Fine-grained particles (mostly < 5 µm, rarely 50–100 µm) were mounted in epoxy resin and solidified within 24 h. The mounted particles were then ground down and polished for subsequent EPMA measurement. Representative chemical compositions of the experimental minerals are listed in Table 5.

The pH of each suspension was measured before and after the reaction under ambient conditions (Table 4). The liquid samples were analyzed using inductively coupled plasma–optical emission spectrometry (ICP-OES; Agilent 5110). We calculated the fluid speciation of the analyzed fluids, the in situ pH values, and the phase diagram of the SiO_2–CaO–MgO–H_2O system for the experimental P–T conditions (at 275 °C and 5.7 MPa) using the program SOLVEQ (Reed 1982) and thermodynamic data taken from the SUPCRT92 database (Johnson et al. 1992).

Results

Characteristics of carbonated serpentinites from the Manlay ophiolite

The ultramafic body of the Manlay ophiolite (Fig. 1a and b) is completely altered by multi-stage serpentinization, and there are no relics of olivine and pyroxenes (Amarbayar et al. 2021). Serpentinization is characterized by (1) replacement of olivine by lizardite, (2) chrysotile formation after orthopyroxene (bastite) as a replacement for the relic of olivine grains, and (3) chrysotile vein development cutting all previous textures. Carbonation occurs in various ways after serpentinization. One of the typical occurrences of carbonated serpentinite is characterized by intense vein networks that cut the serpentinites (Fig. 1c). The other is a pseudomorphic replacement consisting of carbonates and quartz, shown as white to yellowish in the outcrop (Fig. 1d). These rocks are commonly completely carbonated. Completely carbonated serpentinite (Fig. 1d) is located around 10 m from the partially carbonated serpentinite outcrop to the south. Trends in carbonation degree in the outcrop scale are not yet fully understood. In the following sections, we describe the detailed mineralogy and microstructures of the partially carbonated serpentinite with intensive veining and the completely carbonated serpentinites with pervasive replacement. The mineral assemblages are listed in Table 1.

Partially carbonated serpentinite with intensive veining

The partially carbonated serpentinite sample consists of serpentine (lizardite and chrysotile), calcite, and a small amount of dolomite, magnetite, diopside, and Cr-spinel (Fig. 3a) but primary olivine and orthopyroxene are absent in these samples. The early-stage serpentine occurred as a mesh texture (mainly lizardite), bastite (chrysotile), and cross-cutting veins (chrysotile) (Fig. 3a). The serpentine grain size and color are ~ 150 µm and colorless, respectively (Fig. 3b and c). Magnetite occurs along with the fractures and is locally associated with Cr-spinel and carbonate minerals (Fig. 3b–g). Cr-spinel has subhedral to anhedral shapes and is 100–500 µm in size (Fig. 3b).

The serpentinite minerals are crosscut by carbonate veins and/or replaced by carbonate minerals. The Raman spectral peaks at 152, 280, and 1085 cm^{-1} indicate that calcite is the dominant carbonate mineral (Fig. S1). The grain size of subhedral to euhedral calcite varies between < 10 and 500 µm but usually appears fine-grained (< 50 µm) and brownish (Fig. 3b). Calcite occurs as patchy and veins, associated with a fine-grained (< 10–50 µm) dolomite vein (Fig. 3b–d). Thin dolomite veins occur parallel to the calcite veins (Fig. 3e–g). In contrast, medium-grained (100–500 µm) calcite replaces the serpentine (Fig. 3). Vein and patchy calcites are connected each with other (Fig. 3a–c). The subhedral to euhedral magnetite size varies between 50 and 200 µm (Fig. 3f). Magnetite is confirmed through reflected light microscopy in conjunction with electron probe micro analyses.

Completely carbonated serpentinite

Two completely carbonated serpentinites (1809130211 and 1,809,130,204) are analyzed in detail. Sample 1809130204 is mainly composed of calcite with minor amounts of serpentine, dolomite, magnetite, and Cr-spinel. Sample 1809130211 cut by later calcite vein (white large calcite vein; Fig. S2b) consists of calcite, quartz, minor dolomite, magnetite, and Cr-spinel (Fig. 4a). In particular, sample 1809130211 shows a concentric zonal structure composed of quartz and carbonates. Dolomite occurs in the center of the zonal texture and is locally associated with calcite (Fig. 4b), which appears as brownish or yellowish owing to fine grains (Fig. 4a). The replacement of calcite + quartz + magnetite occurs as very fine grains and is brownish (Fig. 4a and c). Primary serpentine is completely absent, but the outlines of the

Table 5 Representative chemical compositions of reactant and product minerals in the experiments

Type	Single step		Single step						Two step							
Name	Ol_NaCa		Srp_NaWo						Ol_Carb_Ca							
Step									Step 1				Step 2			
	Initial	Secondary	Initial		after exp		Secondary		Initial	Secondary			Secondary			
Mineral	Ol	Cal	Wol	Srp	Srp	Wol	Qz	Cal	Ol	Srp	Mgs	Mgt	Srp	Cal	Mg-Cal	Mgt
SiO_2	41.03	0.06	51.19	42.03	40.59	51.71	96.90	n.d	40.93	37.44	0.17	1.63	43.27	0.14	0.94	0.34
TiO_2	< 0.01	0.01	n.d	n.d	0.02	n.d	n.d	n.d	< 0.01	0.02	0.03	0.23	n.d	0.03	0.02	0.01
Al_2O_3	< 0.01	0.02	n.d	0.77	0.45	n.d	n.d	n.d	0.01	0.17	n.d	0.11	0.22	0.03	n.d	n.d
Cr_2O_3	< 0.01	0.03	n.d	n.d	0.07	0.02	0.02	n.d	< 0.01	0.03	n.d	n.d	n.d	n.d	0.03	0.03
FeO	8.36	0.08	0.26	2.24	2.61	0.29	n.d	0.05	8.24	5.98	2.17	78.32	3.17	0.17	0.25	88.43
MgO	50.10	0.25	0.01	35.57	36.53	0.01	0.02	0.03	49.98	43.17	44.09	6.22	38.53	0.44	13.88	0.11
MnO	0.11	0.05	0.30	0.01	0.09	0.16	n.d	0.46	0.13	n.d	0.58	0.63	0.01	0.01	0.03	0.02
CaO	0.05	57.28	47.34	0.19	0.10	46.38	0.70	55.94	0.04	0.03	0.29	0.01	0.02	57.30	39.85	n.d
NiO	< 0.01	n.d	n.d	n.d	n.d	n.d	n.d	n.d	0.04	0.34	0.12	n.d	0.03	0.01	n.d	0.01
Na2O	0.07	0.06	n.d	0.08	0.18	n.d	0.04	n.d	0.04	0.04	0.31	n.d	n.d	0.04	0.02	0.18
K2O	0.01	n.d	n.d	0.01	n.d	n.d	n.d	n.d	< 0.01	0.01	< 0.01	n.d	n.d	n.d	n.d	n.d
Total	99.72	57.83	99.11	80.93	80.63	98.59	97.69	56.46	99.42	87.22	47.75	87.16	85.25	58.18	55.02	89.12
Ox	4	1	6	7	7	6	–	1	4	7	1	4	7	1	1	4
Si	1.001	< 0.01	2.00	2.09	2.04	2.02	–	n.d	1.001	1.808	< 0.01	0.06	2.059	< 0.01	0.144	0.01
Ti	< 0.01	< 0.01	n.d	n.d	< 0.01	n.d	–	n.d	< 0.01	< 0.01	< 0.01	< 0.01	n.d	< 0.01	< 0.01	< 0.01
Al	< 0.01	< 0.01	n.d	0.05	0.03	n.d	–	n.d	< 0.01	< 0.01	n.d	< 0.01	0.012	< 0.01	n.d	n.d
Cr	< 0.01	< 0.01	n.d	n.d	< 0.01	< 0.01	–	n.d	< 0.01	< 0.01	n.d	n.d	n.d	n.d	< 0.01	< 0.01
Fe^{3+}	–	–		–	–	–	–	–	–	–	–	1.855	–	–	–	1.985
Fe^{2+}	0.171	< 0.01	< 0.01	0.09	0.11	< 0.01	–	< 0.01	0.168	0.242	0.03	0.689	0.126	< 0.01	< 0.01	0.979
Mg	1.822	< 0.01	< 0.01	2.64	2.74	< 0.01	–	< 0.01	1.823	3.108	0.95	0.36	2.734	< 0.01	0.315	< 0.01
Mn	< 0.01	< 0.01	< 0.01	< 0.01	< 0.01	< 0.01	–	< 0.01	< 0.01	n.d	0.01	0.02	< 0.01	< 0.01	< 0.01	< 0.01
Ca	< 0.01	0.988	1.98	0.01	< 0.01	1.94	–	0.99	< 0.01	< 0.01	< 0.01	< 0.01	0.012	0.980	0.651	n.d
Ni	n.d	n.d	n.d	n.d	n.d	n.d	–	n.d	< 0.01	< 0.01	< 0.01	n.d	< 0.01	< 0.01	n.d	< 0.01
Na	< 0.01	< 0.01	n.d	< 0.01	0.02	n.d	–	n.d	< 0.01	< 0.01	< 0.01	n.d	n.d	< 0.01	< 0.01	0.01
K	< 0.01	n.d	n.d	< 0.01	n.d	n.d	–	n.d	< 0.01	< 0.01	< 0.01	n.d	n.d	n.d	n.d	n.d
Mg#	0.92	–	–	0.97	0.96	–	–	–	0.92	0.93	0.99	0.34	0.96	–	–	0.01
Ca#	–	0.99	–	–	–	–	–	0.99	–	–	–	–	–	0.99	0.67	–

Ol livine, *Srp* serpentine, *Mgs* magnesite, *Cal* calcite, *Mg-Cal* Mg-Calcite, *Wol* Wollastonite, *Mgt* Magnetite, *n.d* not detected

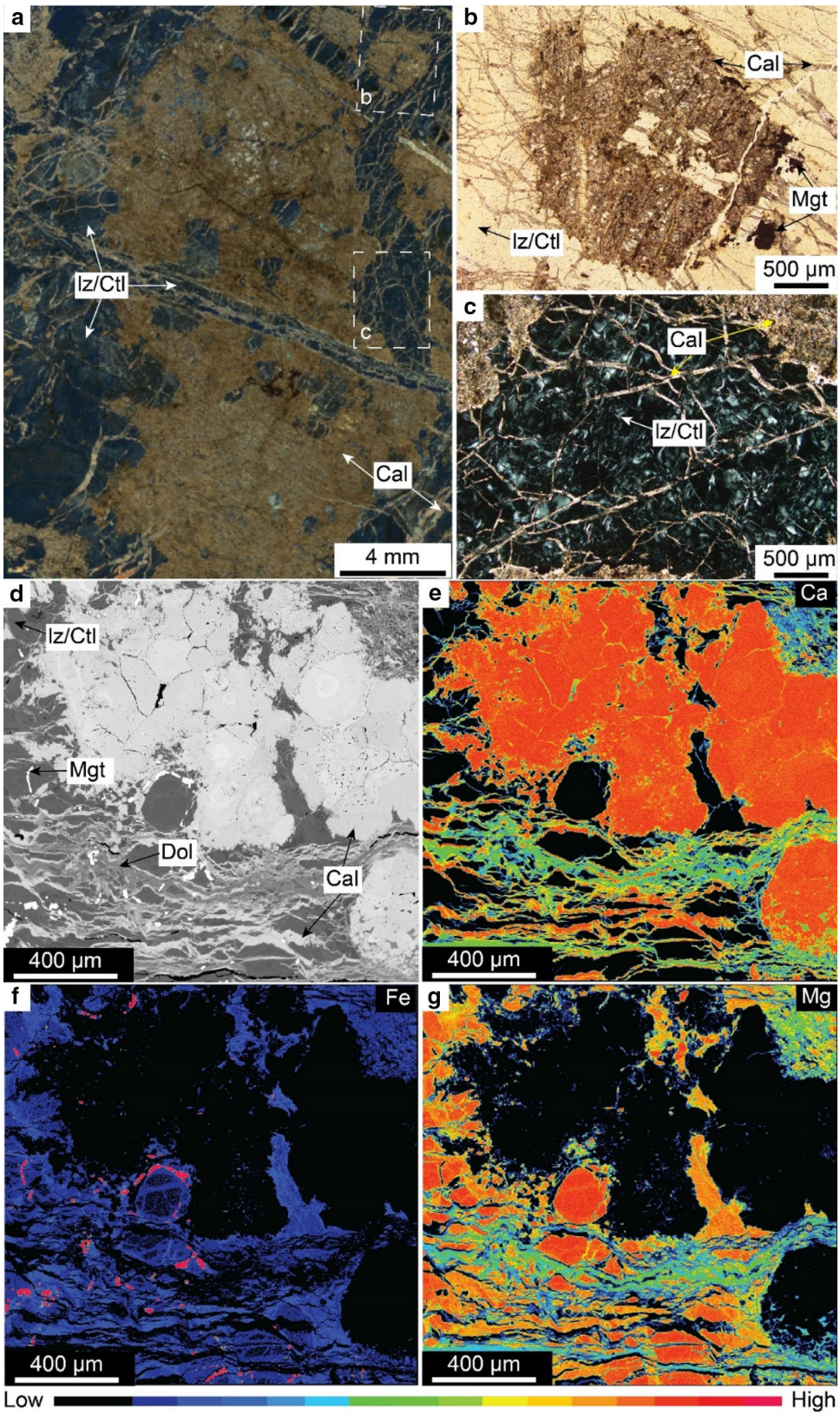

Fig. 3 Microtexture of partially carbonated serpentinite in the Manlay ophiolite. **a** photomicrograph of partially carbonated serpentinite under cross-polarized light (xpl). Dashed rectangles indicate areas of (**b**) and (**c**). **b** photomicrograph of serpentine, and patchy and vein calcites under plane-polarized light (ppl). Serpentines are partially replaced by calcite. **c** photomicrograph of vein network of calcite in the serpentinite under xpl. Vein calcite is connected to patchy calcite. **d** BSE image of patchy and vein calcite. Coarse-grained calcite replaced the serpentine, and fine-grained calcite incorporated replacement and vein formation. Vein calcite coexisted with dolomite. **e** Ca mapping of (**d**) clearly shows the distribution of dolomite and calcite as green and orange-red, and green colors, respectively. (**f**) Fe mapping of (**d**) exhibits magnetite and serpentine distribution as red and blue colors, respectively. **g** Mg mapping of (**d**) displays the distribution of serpentine and dolomite as orange-red and green colors, respectively. *Lz* lizardite, *Ctl* chrysotile, *Cal* calcite, *Dol* dolomite, *Mgt Magnetite*

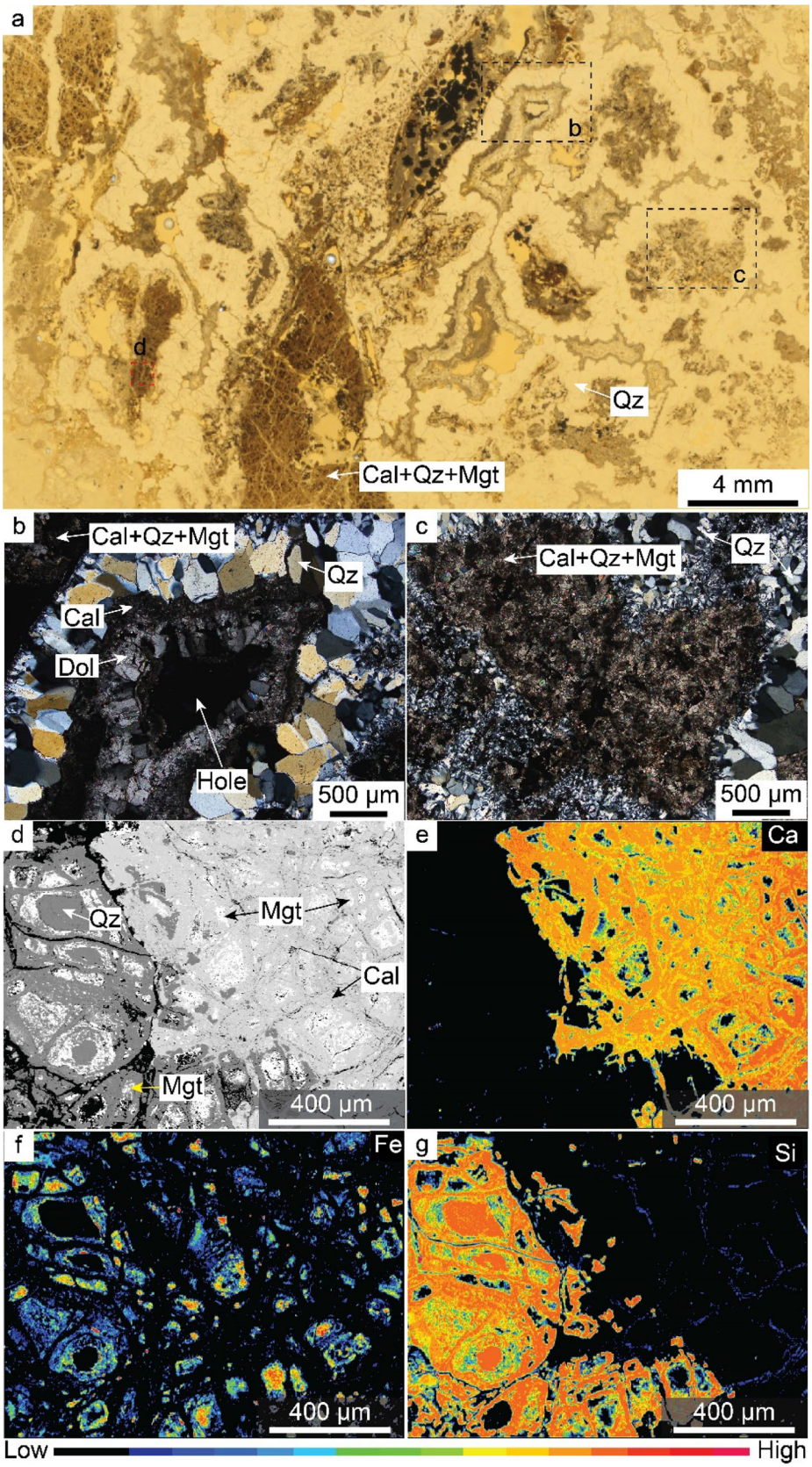

Fig. 4 Microtexture of completely carbonated serpentinite in the Manlay ophiolite. **a** photomicrograph of completely carbonated serpentinite under plane-polarized light (xpl). Dashed black and red rectangles indicate areas of (**b**), (**c**), and (**d**). **b** the photomicrograph of quartz, calcite, and dolomite zonal texture under cross-polarized light (xpl). **c** photomicrograph of replacement composed of calcite, quartz, and magnetite under xpl. Replacement is surrounded by fine- and coarse-grained quartz. **d** The BSE image of the presentative replacement showed a mesh texture consisting of calcite and quartz in the core. A magnetite rim surrounds a core of calcite and quartz. The magnetite rim is surrounded by calcite and quartz. **e** Ca mapping of (**d**) shows that one side of mesh texture is mainly composed of calcite. **f** Fe mapping of (**d**) exhibits that magnetite indicates the location of mesh core remained from serpentinite. **g** Si mapping of (**d**) displays that one side of mesh texture is mainly composed of quartz. *Qz* quartz, *Cal* calcite, *Dol* dolomite, *Mgt* magnetite

mesh texture of serpentine are preserved in the replacement (Fig. 4d). Calcite appears in a subhedral shape and fine-grained (< 50 µm) and is found in the mesh core, rim, and zonal texture (Fig. 4b–f). Elongated quartz occurs in the outer parts of the zonal texture with calcite and dolomite (Fig. 4b) and in the mesh core and rim (Fig. 4g). The grain size of the quartz varies between 10 and 500 µm (Fig. 4b and c). The Raman spectral peaks at 122, 200, and 458 cm^{-1} confirm the presence of quartz (Fig. S1), whereas 170, 297, 720, and 1100 cm^{-1} are the representative peaks of dolomite (Fig. S1). Fine-grained (< 10–100 µm) magnetite occurs as the rim of the mesh texture and is associated with carbonate minerals (Fig. 4d and f). Cr-spinel has anhedral to subhedral shapes, is 10–300 µm in size (mostly < 100 µm), and often rimmed by magnetite.

Mineral chemistry

The serpentine minerals in partially carbonated samples (Table 1) show moderately high Fe content with Mg# from 0.87 to 0.98, and has relatively elevated Al_2O_3 (0.15–3.45 wt%), Cr_2O_3 (< 1.74 wt%) and NiO (< 0.64 wt%) contents in comparison with the serpentines of the serpentinite samples (Amarbayar et al. 2021). Cr-spinel in the partially carbonated serpentinite has Cr# [= Cr/(Al + Cr)] and Mg# [= Mg/(Mg + Fe^{2+})] ranging from 0.55 to 0.59 and from 0.45 to 0.54, respectively (Fig. 5a). Cr-spinel in the completely carbonated serpentinite has Cr# and Mg# ranging from 0.83–0.84 and from 0.32–0.35, respectively (Fig. 5a). Calcite in partially and completely carbonated serpentinites shows a chemical composition of 55.26–56.48 wt% CaO, 0.42–0.97 wt% MgO, and < 0.01–0.08 wt% MnO contents, whereas dolomite has 29.94–30.66 wt% CaO

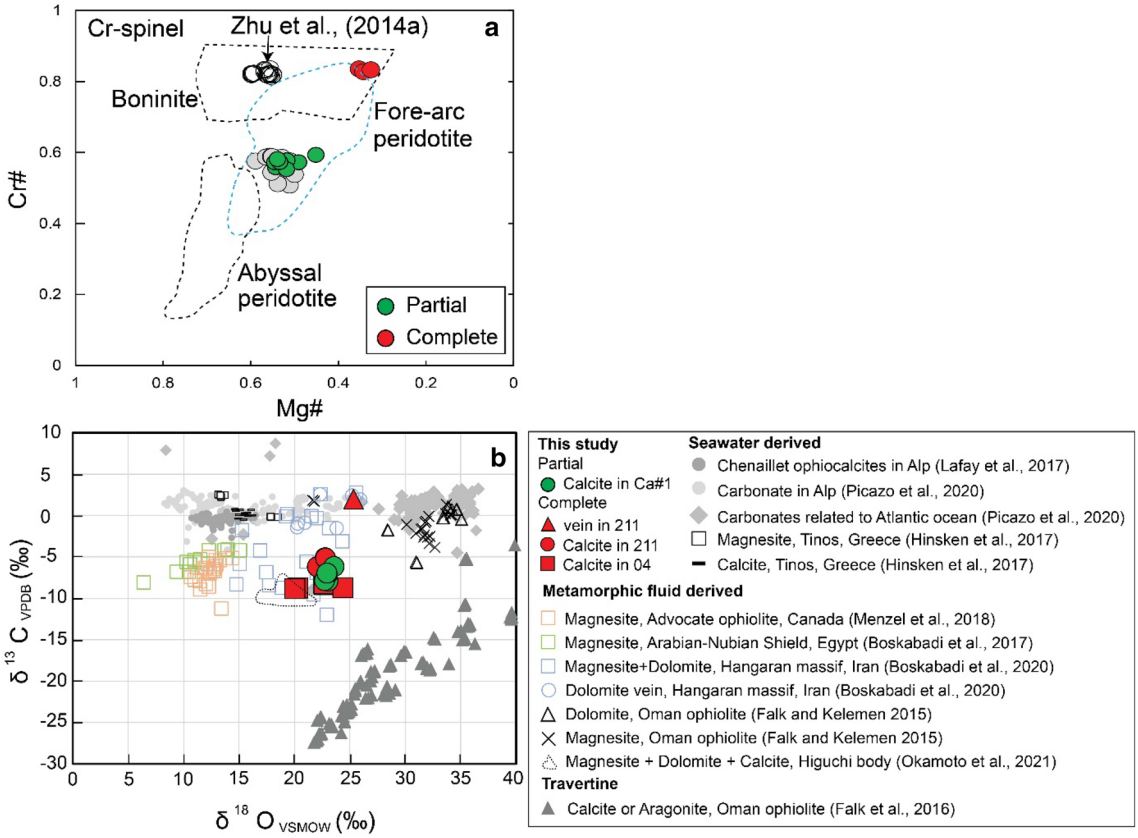

Fig. 5 **a** Mg# vs. Cr# plot of chromian spinels of partially carbonated serpentinite (green circle) and completely carbonated serpentinite (red circle). Chromian spinels in Chromitite (green) from Zhu et al. (2014) and in serpentinites from Amarbayar et al., (2021) are shown as open and gray circles, respectively. Areas of Abyssal peridotite, Fore-arc peridotite, and Boninitite are from Tamura and Arai (2006). **b** Isotopic compositions ($\delta^{13}C_{VPDB}$ and $\delta^{18}O_{SMOW}$) of calcite in partially and completely carbonated serpentinites of the Manlay ophiolite. Chenaillet ophiocalcites in Alp are from Lafay et al. (2017); Carbonate in Alp are from compiled data of Picazo et al. (2020); magnesite and calcite, Tinos, Greece are from Hinsken et al. (2017); magnesite in the Advocate ophiolite, Canada is from Menzel et al. (2018); magnesite in the Arabian-Nubian Shield, Egypt is from Boskabadi et al. (2017); magnesite + dolomite and dolomite vein in the Hangaran massif, Iran are from Boskabadi et al., (2020); carbonate of the Higuchi serpentinite in the Sanbagawa belt, Japan is from Okamoto et al. 2021; carbonates in the Oman ophiolite are from Falk and Kelemen (2015) and Travetine data is from Falk et al. (2016)

and 19.90–22.00 wt% MgO contents (Table 2). Calcite has $X_{Mg,cal}$ [= Mg/(Mg + Fe + Ca)] value 0.015–0.023, whereas dolomite has $X_{Fe,dol}$ [= Fe/(Mg + Fe)] value less than 0.01.

Cr-spinel has Cr# and Mg# in the completely carbonated samples ranging from 0.83 to 0.84 and from 0.33 to 0.35, respectively (Fig. 5a). Calcite shows a chemical composition of 61.20–62.36 wt% CaO, 0.45–0.94 wt% MgO, and < 0.01 wt% MnO contents, whereas dolomite has 32.78–35.38 wt% CaO and 20.37–23.88 wt% MgO contents (Table 2). Calcite has $X_{Mg,cal}$ values from 0.01 to 0.021, whereas dolomite has $X_{Fe,dol}$ values less than 0.002. Magnetite has FeO_{total} (84.46–91.20 wt%) content and slightly high SiO_2 (0.04–0.69 wt%) and MnO (< 0.59 wt%) contents (Table 2).

Carbon and oxygen isotope compositions

A total of 16 C–O isotope analyses of calcites from one partially carbonated serpentinite (18091302Ca01) and two completely carbonated serpentinites (1809130211 and 1809130204) is performed in this study (Table 3 and Fig. 5b). Calcite from a partially carbonated serpentinite (18091302Ca01) has fairly constant values of $\delta^{13}C_{VPDB}$ (from − 7.92 to − 6.16 ‰) and $\delta^{18}O_{VSMOW}$ (from + 22.7 to + 23.6 ‰) whereas calcite from a completely carbonated serpentinite (1809130211) is characterized by a relatively constant value of $\delta^{13}C_{VPDB}$ (from − 6.19 to − 5.11‰) and $\delta^{18}O_{VSMOW}$ (from + 22.1 to + 22.8‰), except for the later calcite vein (white large calcite vein; Fig. S2b), which has a value of $\delta^{13}C_{VPDB}$ (+ 1.97‰) and $\delta^{18}O_{VSMOW}$ (+ 25.3 ‰). Calcite in sample 1809130204 (completely carbonated serpentinite) displays relatively low $\delta^{13}C_{VPDB}$ value (from -8.83 to -8.27 ‰) and a relatively wide range of $\delta^{18}O_{VSMOW}$ (from + 20.1 to + 24.4 ‰).

Results of hydrothermal experiments

Single step experiment on Olivine + $NaHCO_{3,aq}$ + $CaCl2_{,aq}$ (no. Ol_NaCa)

After the experiments with HCO_3^- and Ca^{2+}, olivine alteration, and calcite precipitation occurs simultaneously. According to the XRD analysis of the reacted solid samples, the calcite peak is dominant, a minor amount of serpentine is generated, and some olivine remains after 48 h of reaction (Fig. 6a). The XRD or SEM observations do not detect magnesite, magnetite, or brucite. Calcite occurs as euhedral crystals with the size of 10–150 µm and has no spatial relationship with olivine grains. Serpentine occurs as a fine-grained aggregate surrounding the relics of olivine grains (Fig. 6b). This indicates that a large amount of calcite is generated directly from a reaction between

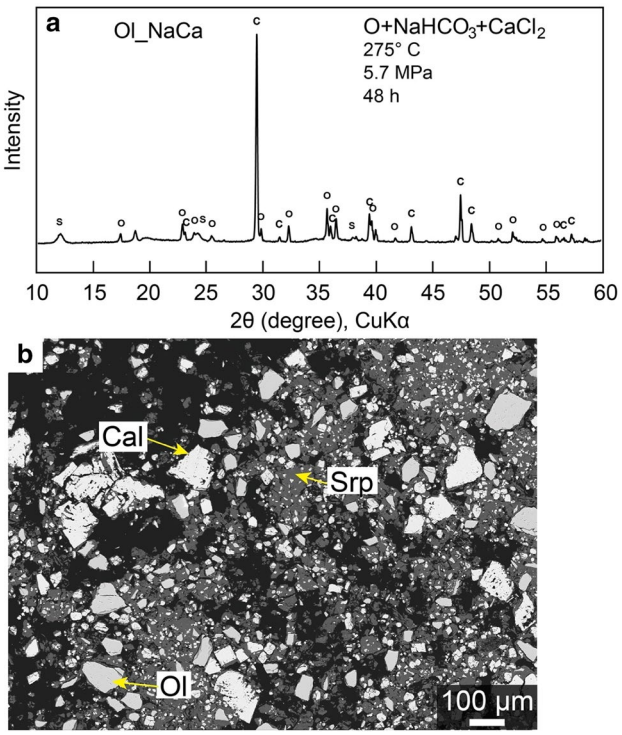

Fig. 6 A single step experiment (Ol_NaCa) in which carbonated olivine reacted with 0.7 mol/L $CaCl_2$ for 56 h at 275 °C and 5.7 MPa. **a** XRD pattern of experiment 2. *S* serpentine, *C* calcite, *W* wollastonite. **c** BSE image of reacted olivine and produced serpentine and calcite. Parent olivine remains. Calcite and serpentine are generated. *Ol* Olivine, *Srp* serpentine, *Mgt* magnetite, *Cal* calcite

HCO_3^- and Ca^{2+} without being included in the olivine hydrothermal reactions.

Single step experiment on Chrysotile + $NaHCO_{3,aq}$ + wollastonite (no. Ctl_NaWo)

In this experiment, wollastonite is used as the source of Ca, and chrysotile is used as an analog of serpentinized peridotite. The XRD measurement of the reacted solid sample shows strong peaks of calcite and relic of wollastonite and serpentine, but peaks of quartz are not detected (Fig. 7a). SEM observations reveal that in addition to the initial fibrous serpentine minerals and wollastonite, calcite and amorphous silica are also produced (Fig. 7b, c, d, e). Calcite occurs as euhedral crystals of 10–50 µm, and amorphous silica occurs in a shape similar to that of wollastonite or spherical particles (Fig. 7c). The Mg# of chrysotile before and after the experiments is similar (0.964–0.965), and there was no evidence of serpentine dissolution and of magnesite formation (Table 5).

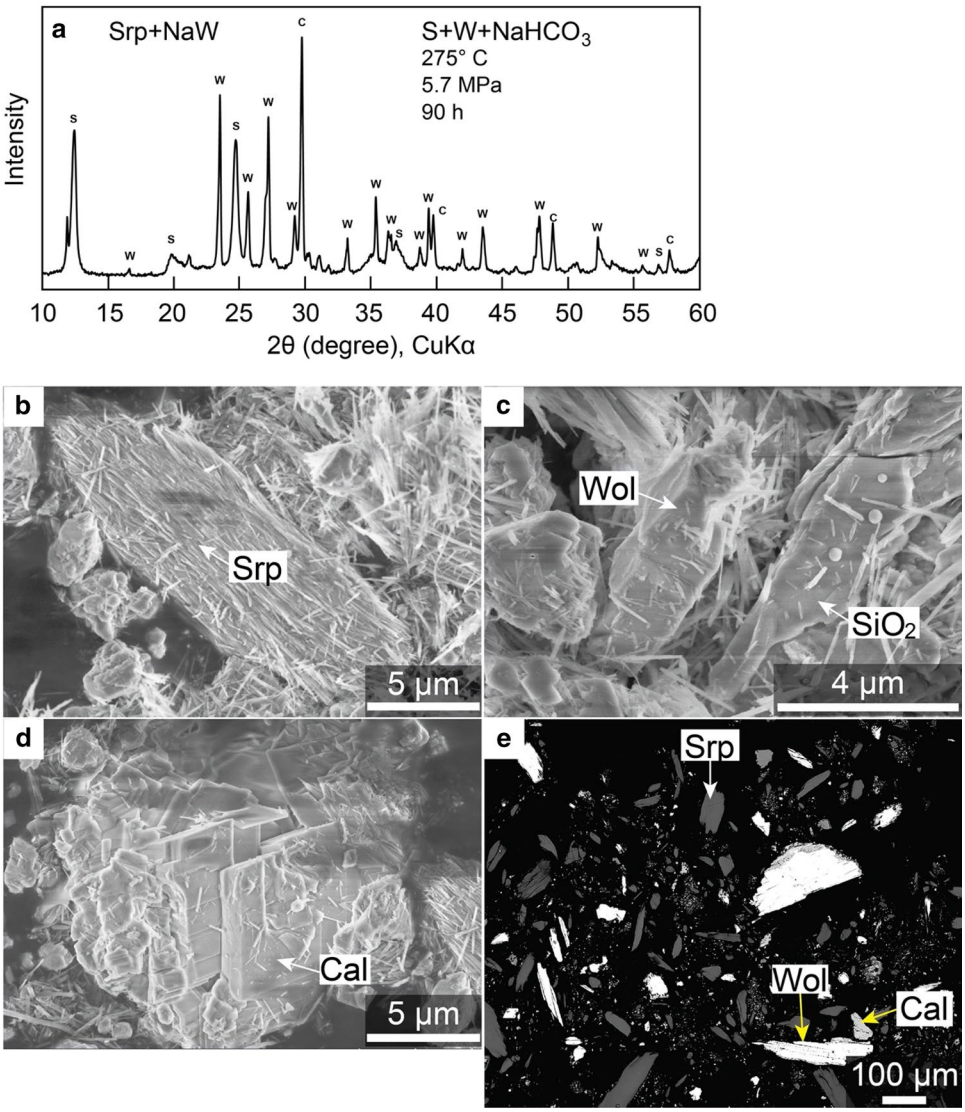

Fig. 7 In a single-step experiment (Serp_NaWo), serpentine and wollastonite reacted with 0.5 mol/L $NaHCO_3$ for 90 h at 275 °C and 5.7 MPa. **a** XRD pattern of experiment 3. *S* serpentine, *C* calcite, *W* wollastonite. **b** needle-like serpentine covers the original serpentine. **c** wollastonite with amorphous silica shows an unreacted shape. **d** calcite displays a clear rhombohedral shape. **e** BSE image of parent serpentine and wollastonite and produced calcite. Serpentine shows an unreacted surface, whereas wollastonite exhibits reacted surface. *Srp* serpentine, *Cal* calcite, *Wol* wollastonite

Two-step experiment of olivine carbonation and Ca-metasomatism (Ol_Carb_Ca)

Step 1: Olivine carbonation ($Ol + NaHCO_{3,aq}$)

According to the XRD measurements, the solid samples at this stage contain substantial amounts of serpentine (e.g., peaks at 12.1°, 23.9°, and 38.3°) and magnesite (e.g., peaks at 32.6° and 38.9°), and some olivine remains (Fig. 8a). Chrysotile is the dominant serpentine species with a monoclinic or tubular shape, and the length of the chrysotile is less than 1 μm. The surface of the reacted olivine is partially covered by these chrysotiles (Fig. 8b). In addition, magnetite (~6 μm) exists as euhedral crystals with an octahedral shape (Fig. 8c). A rhombohedral shape of the magnesites is observed, and the size varied between 2 and 70 μm (Fig. 8d). The average mineral composition is listed in Table 5. The average Mg# of the secondary serpentine is ~0.93, similar to that of olivine (0.91). Magnesite (Mg# = 0.99) and serpentine are observed along with the remaining olivine particles (Fig. 8e).

Step 2: Ca-metasomatism (Products of step 1 + $CaCl_{2,aq}$)

After step 2, the XRD spectra suggests that the amount of serpentine increases (Fig. 9a), indicating that the partially reacted olivine is further hydrated at this stage. This result is consistent with the SEM observation that the olivine surface is fully covered by serpentines (Fig. 9b). The serpentines have an average Mg# of 0.96, which is relatively high compared to that obtained after Step 1 (Mg# = 0.93; Table 5). The amount of magnetite (3–13 μm) is higher than that in Step 1 (Fig. 9c).

Interestingly, the magnesite peaks are reduced and almost disappeared at this stage, whereas calcite peaks appeared (Fig. 9a). Consistently, magnesite particles are not observed in the SEM observations, and calcite occurs as a pseudomorphic replacement for magnesite (~4 μm; Fig. 9d). Calcite bands (+ locally magnetite) with median lines of Mg-calcite

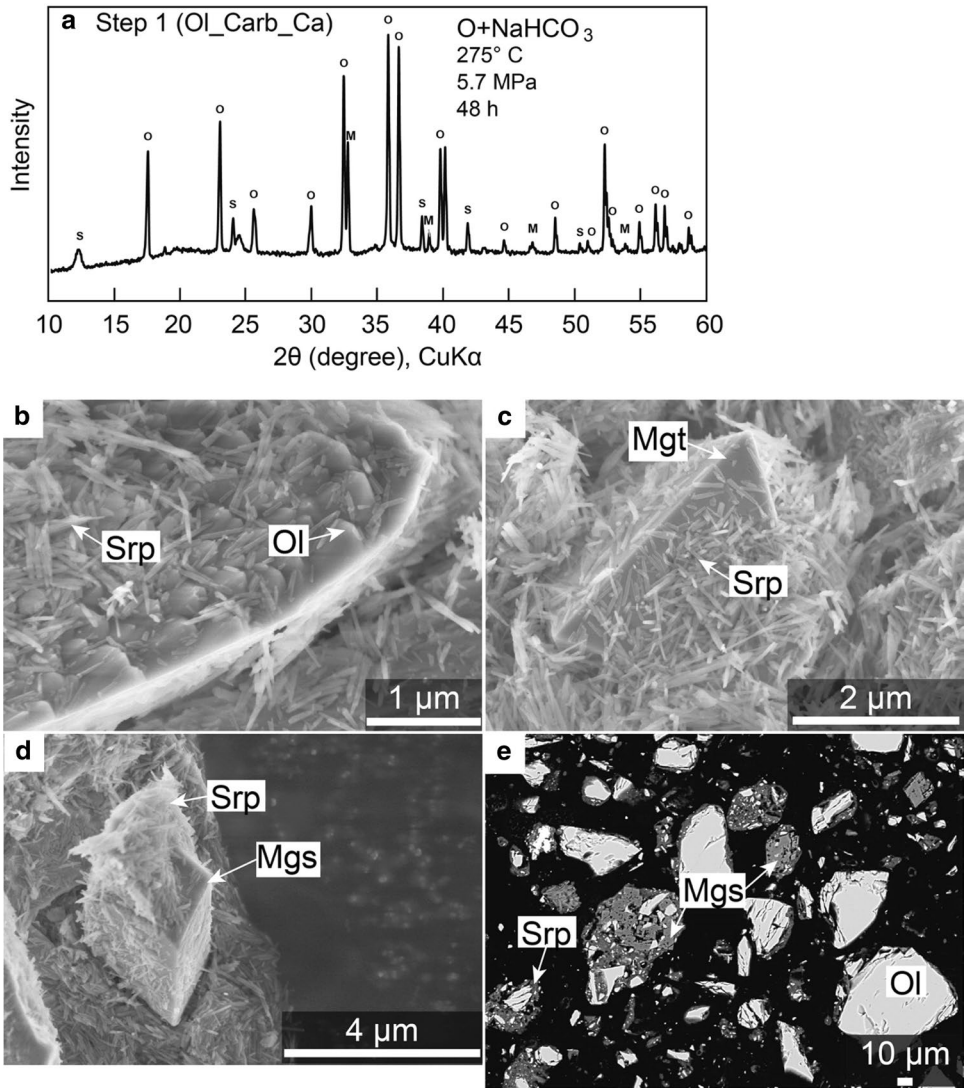

Fig. 8 Step 1 experiment of two step-experiment (*Ol_Carb_Ca*) in which olivine reacted with 0.5 mol/L $NaHCO_3$ for 48 h at 275 °C and 5.7 MPa. **a** X-ray powder diffraction (XRD) pattern of experiment 1.1. *O* Olivine, *S* serpentine, *M* magnesite. **b** Olivine surface covered by needle-like serpentine. **c** Magnetite with serpentine exhibits an octahedral shape. **d** Magnesite with serpentine shows a rhombohedral shape. **e** BSE image of serpentine and magnesite formed from olivine and remained initial olivine after the reaction. *Ol* Olivine, *Srp* serpentine, *Mgt* magnetite, *Mgs* magnesite

occurs locally, which cut the serpentine clasts (Fig. 9e). This banded texture is similar to the natural samples obtained from the Manlay ophiolite in southern Mongolia (Fig. 3d–g).

Solution chemistry at Step 1 and Step 2

The fluid chemistry after Steps 1 and 2 is shown in Table 4. The initial solution of Step 1 ($NaHCO_3$ aqueous solution) does not contain Mg, Si, K, Ca, or Mn. After Step 1, the pH at room temperature (around 25 °C) is 8.8, close to the initial value (pH = 8.2). The Mg is 2.0 ppm, Si is 4.8 ppm, and K is 8.2 ppm. The Ca and Mn concentrations are less than 1 ppm.

After Step 2, the pH at room temperature is 7.4, which decreased from the initial value in Step 2 (pH 9.4). Ca concentration is significantly decreased from 28,000 ppm (0.7 mol/L) to 6226 ppm. In contrast, the Mg concentration is increased significantly from 2 to 195 ppm, suggesting the potential replacement of Mg in magnesite by Ca, which is also evidenced by the significant decrease in Ca concentration. The Si concentration is decreased from 4.8 ppm to 0.6 ppm.

Discussion

Carbonation of ultramafic rocks in the Manlay ophiolite

The outcrop occurrences and microstructures of the ultramafic rocks from the Manlay ophiolite indicate that carbonation occurred after serpentinization; however, the occurrences of carbonates varied. In the partially carbonated serpentinite sample, calcite and dolomite veins cut the initial textures of the serpentines (Fig. 3d). In contrast, calcite, quartz, and magnetite in a completely carbonated

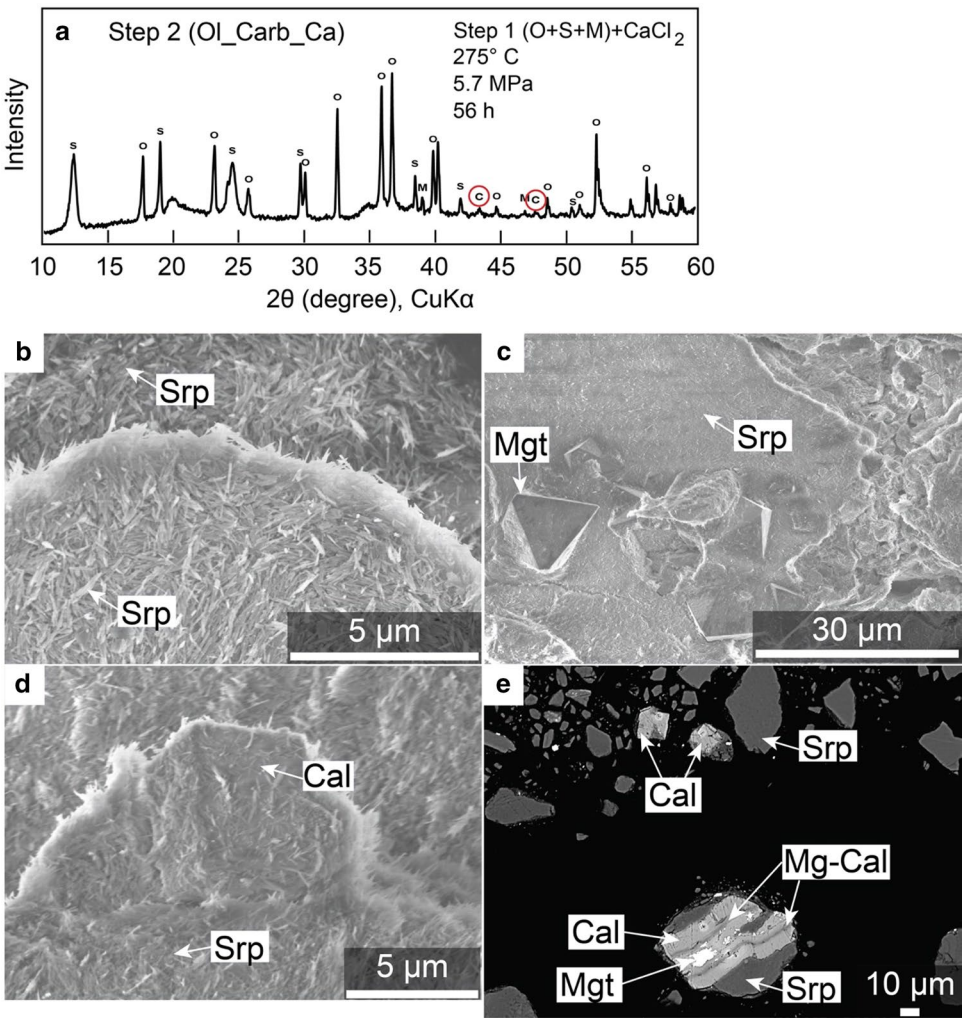

Fig. 9 Step 2 experiment of two step-experiment (Ol_Carb_Ca) in which carbonated olivine reacted with 0.7 mol/L $CaCl_2$ for 56 h SEM images of experiment 1 and 3 at 275 °C and 5.7 MPa. **a** X-ray powder diffraction (XRD) pattern of experiment 1.2. Red circles indicate diffraction pattern of calcite replacing magnesite. *O* Olivine, *S* serpentine, *M* magnesite, *C* calcite. **b** serpentine shows needle-like shape. **c** magnetite displays clear octahedral shape. **d** calcite with needle-like serpentine does not manifest a clear shape. **e** Calcite and Mg-calcite formation after reaction. *Srp* serpentine, *Mgt* magnetite, *Cal* calcite

sample preserved the outline of the mesh texture, indicating that carbonate and quartz completely replaced the serpentines (Fig. 4d–g). Cr-spinel showed different Cr# in partially (Cr# = 0.55–0.59; possible protolith was harzburgite) and completely (Cr# = 0.83–0.84; possible protolith was dunite) carbonated samples, likely reflecting the difference in protolith ultramafic rock or modification of Cr# during the extent of hydrothermal alteration (e.g., Kimball 1990; Dandar et al. 2019). One of the important observations of the Manlay ophiolite is that the carbonate minerals were not Mg-Fe-rich carbonate but calcite with a small amount of dolomite. This differs from carbonated ultramafic rocks, where magnesite is formed via olivine, orthopyroxene, and CO_2-bearing fluids (e.g. Boskabadi et al. 2020). The temperature of carbonation of the analyzed serpentinite body was thought to have been below 300 °C, as carbonation occurred after the low-temperature (lizardite/chrysotile) serpentinization (Fig. 3 and Fig. 4; Amarbayar et al. 2021).

The source and compositions of carbonic fluids

Based on the mineralogy, mineral compositions, and microstructures without brucite, Amarbayar et al. (2021) discussed that serpentinization of the ultramafic rocks of the Manlay ophiolite proceeded via infiltration of silica-rich fluids at shallow levels of the mantle wedge (< 300 °C). Based on present isotopic data of calcite, below, we discuss possible sources for carbonic fluids which cause carbonation after serpentinization of ultramafic rocks within the Manlay ophiolite.

Figure 5b summarizes the C–O– stable isotopes of the carbonate minerals related to the ultramafic rocks in various occurrences and geological settings. Carbonates derived from seawater have δ^{13} C values close to zero (carbonate in Alps = − 4.14 to + 2.75‰; carbonate in Atlantic ocean = − 4.5 to + 8.7‰; and carbonate from Tinos = − 0.5 to + 2.44‰) alongside a wide variation of δ^{18} O (carbonate in Alps = + 8.54 to + 25.33 ‰; carbonate in Atlantic ocean = + 8.4 to + 36.6‰; and carbonate

from Tinos = + 13.3 to + 18.51 ‰) (e.g., Hinsken et al. 2017; Lafay et al. 2017; Picazo et al. 2020). The carbonates sourced from alkaline spring such as travertine in association with ultramafic rocks showed a positive correlation between δ^{13} C (− 27 to − 3.8 ‰) and δ^{18} O (+ 22 to + 40 ‰) (e.g., Streit et al. 2012; Falk et al. 2016; Christensen et al. 2021). The carbonates sourced from metamorphic fluid varied both in δ^{13} C and δ^{18} O; for example, δ^{13} C = − 11.25 to − 5.3‰ and δ^{18} O = 10.67–14.43‰ for Advocate ophiolite (Menzel et al. 2018), δ^{13} C = − 8.1 to − 4.2 ‰ and δ^{18} O = 6.4–15.1‰ for Arabian-Nubian Shield (Boskabadi et al. 2017), δ^{13} C = − 8.31 to − 2.78‰ and δ^{18} O = 14.77–25.58‰ for Hangaran massif (Boskabadi et al. 2020), δ^{13} C = − 5.71–0.71‰ and δ^{18} O = 28.47–35.09‰ for the listvenite from the Oman ophiolite (Falk and Kelemen 2015), and δ^{13} C = − 10.3 to − 9.3‰ and δ^{18} O = 17.0–20.2‰ for the carbonated serpentinite from the Sanbagawa metamorphic belt (Okamoto et al. 2021).

In the Manlay ophiolite, the later-stage calcite vein has values of δ^{13} C (+ 1.97‰), which are similar to those of typical marine limestones (from − 0.2‰ to 2.9‰; Wada and Suzuki 1982) and marble from the high-pressure metamorphic belt (from 0.4‰ to 2.8‰; Morohashi et al. 2008; Okamoto et al. 2021; Fig. 5c). In contrast, the stable C isotope compositions of calcite in the common carbonate minerals within the serpentinite from the Manlay ophiolite display a range of δ^{13} C (from − 5.1 to − 8.8‰). This value is not marine limestone but could be comparable to the metamorphic fluids in the previous studies from Advocate ophiolite, Arabian-Nubian Shield, the Hangaran massif and the Sanbagawa belt (Fig. 5b; Menzel et al. 2018; Boskabadi et al. 2017, 2020; Okamoto et al. 2021). The stable O isotope compositions of calcite in the partially and completely carbonated serpentinite from the Manlay ophiolite show a relatively wide range of δ^{18} O between + 20.1‰ and + 24.4‰, and this value was comparable to carbonate veins derived from metamorphic fluid in previous literatures (from + 17‰ to + 24‰; Boskabadi et al. 2020; Okamoto et al. 2021). In summary, the C–O isotope values of carbonates from the ultramafic body in the Manlay ophiolite indicate that the carbonic fluids were not originated from the seawater, but probably originated from the fluids related to the metamorphic reactions. The relatively low δ^{13} C values (from − 5.1 to − 8.8‰) and a variation of (from + 20.1‰ to + 24.4‰) of carbonates in the Manlay ophiolite suggests that (1) the possible sources of CO_2 fluids being the degradation of organic material or methanotrophic processes within subducted sediments, and (2) carbonic fluids were mixed with water produced by the dehydration of serpentinite during carbonation or fluid-rock interaction during regional metamorphism, as discussed in previous studies (Bernoulli and Weissert 2021; Okamoto et al. 2021).

Experimental constraints on the mechanism of replacement of ultramafic rocks by calcite

Two types of the single-step experiment (Exp. Ol_NaCa, Exp. Serp_NaWo) using the input of Ca sources and CO_2-bearing aqueous solution, as well as olivine or serpentine, cause a substantial amount of calcite precipitation (Figs. 6 and 7). Despite Mg-bearing mineral in ultramafic rocks (olivine in Exp. Ol_NaCa; serpentine in Exp. Serp_NaWo) were used as input minerals, these experiments did not produce magnesite. Olivine was changed to serpentine in the run Ol_NaCa, and no changes were observed for chrysotile (Serp_NaWo). These results indicate that the reactions between Ca^{2+} ions and HCO_{3^-} ions were much faster than the dissolution of olivine and serpentine, and that if external Ca^{2+}- and CO_2-bearing fluids exist along the fractures, calcite precipitation will immediately occur within the fractures. In the experimental products, the replacement texture after serpentinite was not observed, which is inconsistent with the observations of the Manlay ophiolite.

The Serp_NaWo experiment shows that calcium pyroxene (wollastonite) can be a potential calcium source for calcite formation (Fig. 7a and e). The reaction of Ca-pyroxene to produce carbonate minerals was much faster than that of serpentine (Table 5). In the case of Serp_NaWo, the observed silica phase was amorphous silica, but not quartz, as observed in the Manlay ophiolite. Amorphous silica can transform into quartz during aging at high temperatures (Lynne et al. 2005; Amagai et al. 2019). However, pyroxenes are not likely the only Ca source in the Manlay ophiolite, as the carbonates showed a replacement texture not only of bastite (after pyroxenes) but also after serpentine mesh textures (Fig. 4).

In contrast, the replacement texture of olivine by calcite can be reproduced by a two-step experiment: magnesite + serpentine was formed after olivine at the initial infiltration of carbonic fluids, and magnesite was transformed into calcite by infiltration of $CaCl_2$ fluids (Figs. 2 and 9a). It is noted that serpentine minerals did not react in Step 2 because of the sluggish reactions of serpentine carbonation compared to brucite carbonation (Kelemen et al. 2011).

The change in the solution chemistry is consistent with the mineralogical change during the reaction; in Step 2, Mg^{2+} ions were released from magnesite to the solution during replacement by calcite (Table 4). Figure 10 shows the activity diagram of Ca^{2+} and Mg^{2+} and the stability of magnesite, dolomite, and calcite (Fig. 10). The speciation calculation of aqueous species under in situ conditions in Steps 1 and 2 reveals that magnesite is stable in the solution after Step 1. During Step 2, the solution evolves from the calcite stability field to the region close to the calcite + dolomite stable boundary (Fig. 10). The changes in the solution chemistry during Step 2 represent the decrease in Ca

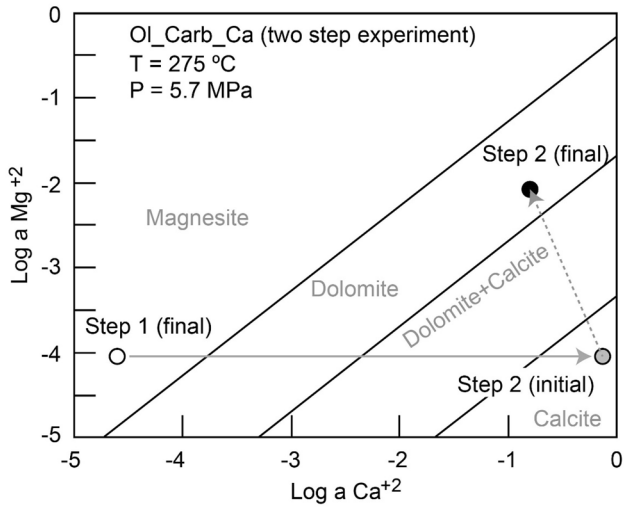

Fig. 10 Plot of log Mg^{2+} vs. log Ca^{2+} in the MgO-CaO-H_2O-CO_2 system at 275 °C and 5.7 MPa for a two-step experiment (Ol_Carb_Ca). Open, grey, and black circles indicate Step 1 (final solution), Step 2 (initial solution), and Step 2 (final solution), respectively

concentration and increase in Mg concentration during the replacement of magnesite with calcite, which is consistent with the occurrence of Mg-calcite within the calcite grains (Fig. 9e).

The occurrence of Mg-calcite veins inside the calcite grain has a texture similar to that of dolomite inside the calcite vein observed in the natural carbonated ultramafic rocks of the Manlay ophiolite (Fig. 3d and 4b). Previous experimental studies have shown that calcite is replaced by dolomite and magnesite through reaction with Mg-rich fluid (e.g., Jonas et al. 2015, 2017; Weber et al. 2021). In contrast, step 2 of the two-step experiments in this study showed that the formation of calcite via the interaction of magnesite and Ca-rich fluid can occur easily in hydrothermal environments (Fig. 9a). Although the magnesite did not remain in the products of Step 2 (Fig. 9b), the texture of calcite at Step 2 (Fig. 9d, e) was similar to that of magnesite at Step 1 (Fig. 8d, e). Such occurrences of magnesite and calcite supported the hypothesis that the formation of calcite occurs via the replacement of pre-existing magnesite

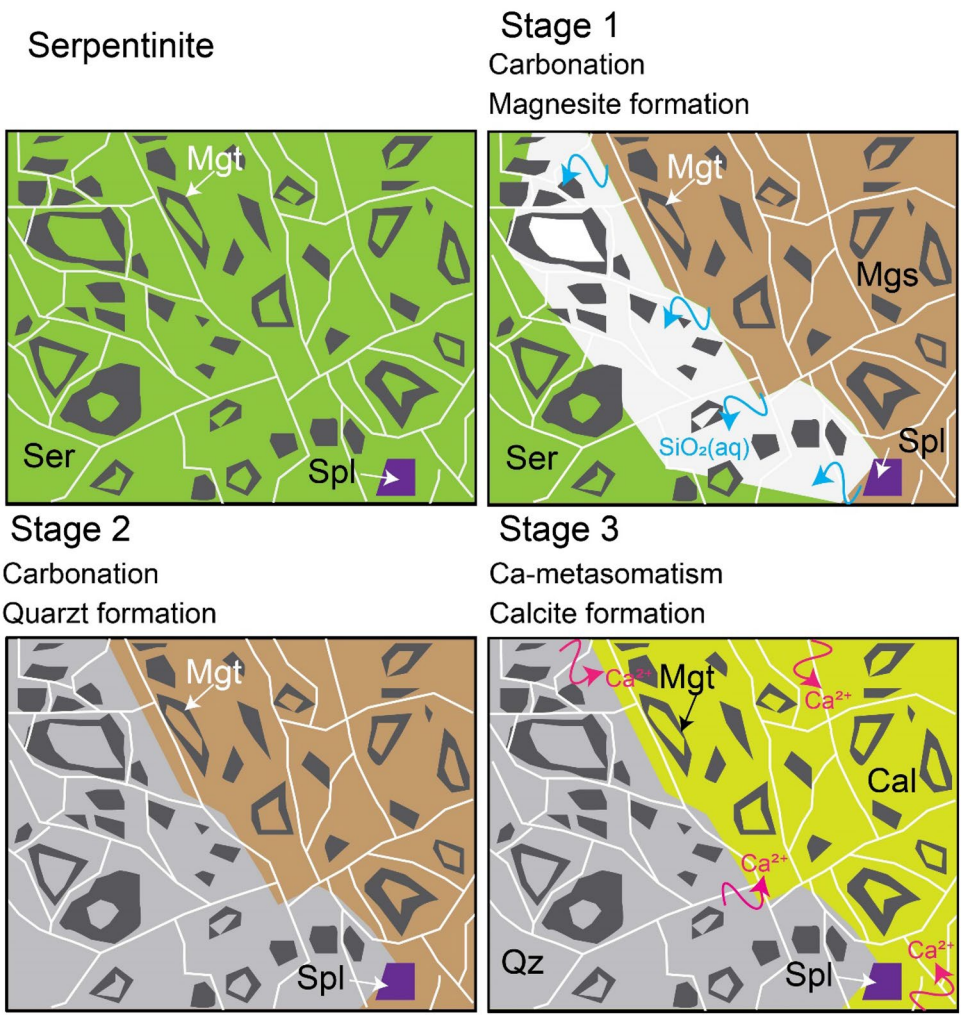

Fig. 11 Microtexture evolution during carbonation of ultramafic rocks in the Manlay ophiolite

via coupled dissolution and precipitation processes (Putnis 2009), as found in the replacement of calcite by magnesite (e.g., Andreani et al. 2009; Jonas et al. 2015, 2017; Weber et al. 2021). The results of the single step experiments revealed that when the aqueous fluids contained both Ca^{2+} and HCO_3^- (or CO_3^{2-}) in high concentrations, calcite directly precipitated from the fluids without reacting with Mg-bearing minerals such as serpentine, olivine, or brucite. Such a situation is comparable to the calcite precipitation in fractures hosted by ultramafic rocks (e.g., Falk and Kelemen 2015; de Obeso and Kelemen 2018). However, such a process would have difficulty in producing the replacement textures of the carbonated serpentinite observed in this study (Fig. 4). Alternatively, the two-step experiment may explain the observed features of natural samples, although the possibility of the direct replacement of serpentinite by calcite cannot be ruled out, whilst we are aware that further experiments covering a large range of possible conditions are necessary to exclude alternative explanations.

In summary, the results of hydrothermal experiments suggest that the pervasive calcite observed in the ultramafic rocks of the Manlay ophiolite could be related to a two-stage alteration process, that is, Ca-rich fluid infiltration after the carbonation of serpentinite.

Multi-stage alteration of ultramafic rocks in the Manlay ophiolite, south Mongolia

Based on the serpentinites that were carbonated by calcite and dolomite alongside the results of the hydrothermal experiments, we propose that calcite was more likely to have been formed by Ca-rich fluid infiltration (the Ca metasomatism) after the main stage of carbonation of ultramafic rock as follows.

Stage 0: Before infiltrating the CO_2 fluids, the ultramafic body was completely serpentinized by developing mesh textures (Amarbayar et al. 2021).

Stage I: Initial carbonation of serpentinite. Serpentinite can react with the CO_2-rich fluid to generate magnesite (Eq. 3; Fig. 8). In the earlier stages, the CO_2 fluids mainly flowed along the fracture networks, but more pervasively to cause uniform replacements of carbonates and quartz. The preservation of the mesh texture recognized the pseudomorphic replacement of serpentine with carbonate (Fig. 4d–g).

Stage II: With the progress of carbonation of serpentinites, silica and water were released from serpentinites (composed of serpentine minerals, brucite, and a relic of pyroxenes) as follows:

$$\begin{aligned} &Mg_3Si_2O_5(OH)_4\,(Ctl/Lz) + 3CO_2 \\ &= 3MgCO_3\,(Magnesite) + 2SiO_2(aq)(Silica) \\ &\quad + 2H_2O\,(Water) \end{aligned} \tag{3}$$

Reaction 3 causes a solid volume decrease of ~ 22% with the molar volume obtained from Holland and Powell (1998). However, predominance of carbonate over quartz in some region of the mesh texture (right half of Fig. 3d) suggest that silica had been mostly removed from such region at least locally. Such removal of silica involves a large volume decrease and could cause fracture (Okamoto et al. 2021) or development of voids (Fig. 4b). The concentric zoning of quartz and carbonates may represent the transport of silica and precipitates within voids. A similar texture to concentric zoning (0.1–1.0 mm) of quartz and carbonates has been reported by Menzel et al. (2022). In stages I and II, we propose that the primary carbonates were magnesite.

Stage III: Ca-rich fluids infiltrated the carbonated serpentinites, and Ca replaced the Mg in magnesite to form calcite (Eq. 4; Fig. 4d and e).

$$MgCO_3\,(Magnesite) + Ca^{2+} = CaCO_3\,(Calcite) + Mg^{2+} \tag{4}$$

This reaction proceeds with dissolution and precipitation, and preserved the original textures of serpentinite. The Mg-calcite or dolomite formed in nature could have been caused by the depletion of Ca^{2+} and an increase in Mg^{2+} during Ca metasomatism.

Significance of Ca-metasomatism of carbonated ultramafic rock

The precipitation of calcite ($CaCO_3$) frequently occurs in contact with spring water or near-surface groundwater (Kelemen and Matter 2008; Ruiz-Agudo et al. 2011), in fractures and pores of peridotite interacting with seawater at the seafloor (Picazo et al. 2020), and in long-lived oceanic hydrothermal systems after serpentinization (Lafay et al. 2017). In contrast to the calcite precipitation in fractures and pores, the results presented here reveal that magnesite can be replaced by calcite during Ca metasomatism of carbonated ultramafic rocks. Therefore, the calcite + quartz assemblage or pervasive calcite precipitation in ultramafic rocks should be addressed with caution. Even now it is difficult to predict (1) where or what conditions Ca-metasomatism occurs under and (2) the origin of Ca for Ca-metasomatism after carbonation without Ca isotope study on calcite.

It is well known that mantle peridotite has the potential for CO_2 storage, and once trapped as carbonates, it is brought into deep subduction zones (Kelemen and Matter 2008; Kelemen and Manning 2015). Magnesite is the most stable mineral at depth in the subduction zone (e.g. Isshiki et al. 2004),

whereas $CaCO_3$ is less stable, and CO_2 is derived from the decomposition of calcite back to the surface (Kerrick and Connolly 2001; Galvez and Pubellier 2019). Therefore, the type of mineralogy (magnesite versus calcite) is essential for the global carbon cycle. The study showed that once the ultramafic rocks were carbonated to form magnesite, they could transform into calcite by infiltrating Ca-rich fluids (Fig. 11). Such later-stage metasomatism of di-variant ions can significantly influence the deep carbon cycle.

Conclusions

1. The ultramafic body within the Manlay ophiolite in Southern Mongolia suffered from multi-stage alteration. Serpentinite (lizardite and chrysotile), with a mesh texture, was partially or completely carbonated. In the partially carbonated samples, intense calcite and dolomite veins cut the serpentinites. In the other samples, serpentinite was completely replaced by calcite and quartz, while preserving the mesh texture. Dolomite is rare, and magnesite is absent.
2. The C-O isotope data from calcite in the partially ($\delta^{13}C_{VPDB}$ = from − 7.92 to − 6.16 ‰; $\delta^{18}O_{VSMOW}$ = from + 22.7 to + 23.6‰) and completely ($\delta^{13}C_{VPDB}$ = from -8.83 to -5.11 ‰; $\delta^{18}O_{VSMOW}$ = from + 20.1 to + 24.4‰) carbonated serpentinites suggest that CO_2 in the fluids is generated from metamorphic fluid rather than the origin of marine limestones.
3. Hydrothermal experiments on serpentinization, carbonation, and Ca-metasomatism resulted that the direct replacement of olivine or serpentine minerals by calcite was hard to occur, whereas that two-step processes is more likely to occur, in which the carbonation of olivine is followed by Ca-rich fluid infiltration to transform magnesite into calcite.
4. The natural occurrences and related hydrothermal experiments had shown the possibility that a two-step process caused the carbonation of serpentinite with calcite in the Manlay ophiolite: carbonation to cause magnesite, and then Ca-metasomatism, which transformed magnesite into calcite.

Supplementary Information The online version contains supplementary material available at https://doi.org/10.1007/s00410-023-02013-z.

Acknowledgements We acknowledged O.Gerel, B.Munkhtsengel, B.Batkhishig, and A.Chimedtseren for introducing us to this field of study and providing advice. We thank Burenjargal Ulziiburen, Manzshir Bayarbold, Kazuki Yoshida, Geri Agroli and Diana Mindaleva for their support during field and laboratory work. We thank Shin-ichi Yamasaki for assisting with ICP-OES analysis at Tohoku University. This research was supported by JSPS KAKENHI Grant Numbers 18KK0376, 22H04932 to A.O, and 21H04937 and JST/JICA SATREPS (no. JPMJSA1703) to N.T.

Author contributions NA designed the overall study under the supervision of NT and AO; NA conducted the experiments and analyzed the results with OD, JW, MU, UB, HT and YI; NA, OD and JW wrote the manuscript, and all authors commented on the manuscript.

Data availability The data that supports the findings of this study are available in the supplementary material of this article.

Declarations

Conflict of interest The authors declare no competing interests.

References

Amagai T, Okamoto A, Niibe T et al (2019) Silica nanoparticles produced by explosive flash vaporization during earthquakes. Sci Rep 9:1–9. https://doi.org/10.1038/s41598-019-46320-7

Amarbayar N, Tsuchiya N, Dandar O et al (2021) Mongolian geoscientist. Mongolian Geosci 53:1–17. https://doi.org/10.5564/mgs.v26i53.1787

Andreani M, Luquot L, Gouze P et al (2009) Experimental study of carbon sequestration reactions controlled by the percolation of CO2-rich brine through peridotites. Environ Sci Technol 43:1226–1231. https://doi.org/10.1021/es8018429

Badarch G, Dickson Cunningham W, Windley BF (2002) A new terrane subdivision for Mongolia: implications for the Phanerozoic crustal growth of Central Asia. J Asian Earth Sci 21:87–110. https://doi.org/10.1016/S1367-9120(02)00017-2

Bernoulli D, Weissert H (2021) Oxygen isotopes in ophicalcites: an ever-lasting controversy? Int J Earth Sci 110:1–8. https://doi.org/10.1007/s00531-020-01934-5

Bjerga A, Konopásek J, Pedersen RB (2015) Talc-carbonate alteration of ultramafic rocks within the Leka ophiolite complex, Central Norway. Lithos 227:21–36. https://doi.org/10.1016/j.lithos.2015.03.016

Boskabadi A, Pitcairn IK, Broman C et al (2017) Carbonate alteration of ophiolitic rocks in the Arabian Nubian Shield of Egypt: sources and compositions of the carbonating fluid and implications for the formation of Au deposits. Int Geol Rev 59(4):391–419. https://doi.org/10.1080/00206814.2016.1227281

Boskabadi A, Pitcairn IK, Leybourne MI et al (2020) Carbonation of ophiolitic ultramafic rocks: listvenite formation in the late cretaceous ophiolites of eastern Iran. Lithos 352–353:105307. https://doi.org/10.1016/j.lithos.2019.105307

Christensen JN, Watkins JM, Devriendt LS et al (2021) Isotopic fractionation accompanying CO2 hydroxylation and carbonate precipitation from high pH waters at the Cedars, California, USA.

Geochim Cosmochim Acta 301:91–115. https://doi.org/10.1016/j.gca.2021.01.003
Dandar O, Okamoto A, Uno M et al (2019) Formation of secondary olivine after orthopyroxene during hydration of mantle wedge: evidence from the Khantaishir Ophiolite, western Mongolia. Contrib Miner Petrol. https://doi.org/10.1007/s00410-019-1623-1
Daval D, Hellmann R, Martinez I et al (2013) Lizardite serpentine dissolution kinetics as a function of pH and temperature, including effects of elevated pCO2. Chem Geol 351:245–256. https://doi.org/10.1016/j.chemgeo.2013.05.020
de Obeso JC, Kelemen PB (2018) Fluid rock interactions on residual mantle peridotites overlain by shallow oceanic limestones: Insights from Wadi Fins, Sultanate of Oman. Chem Geol 498:139–149. https://doi.org/10.1016/j.chemgeo.2018.09.022
Edwards HGM, Villar SEJ, Jehlicka J, Munshi T (2005) FT-Raman spectroscopic study of calcium-rich and magnesium-rich carbonate minerals. Spectrochim Acta Part A Mol Biomol Spectrosc 61:2273–2280. https://doi.org/10.1016/j.saa.2005.02.026
Falk ES, Kelemen PB (2015) Geochemistry and petrology of listvenite in the Samail ophiolite, Sultanate of Oman: complete carbonation of peridotite during ophiolite emplacement. Geochim Cosmochim Acta 160:70–90. https://doi.org/10.1016/j.gca.2015.03.014
Falk ES, Guo W, Paukert AN et al (2016) Controls on the stable isotope compositions of travertine from hyperalkaline springs in Oman: insights from clumped isotope measurements. Geochim Cosmochim Acta 192:1–28. https://doi.org/10.1016/j.gca.2016.06.026
Furnes H, Safonova I (2019) Ophiolites of the Central Asian Orogenic belt: geochemical and petrological characterization and tectonic settings. Geosci Front 10:1255–1284. https://doi.org/10.1016/j.gsf.2018.12.007
Galvez ME, Pubellier M (2019) How do subduction zones regulate the carbon cycle? Cambridge University Press, Cambridge
Grozeva NG, Klein F, Seewald JS, Sylva SP (2017) Experimental study of carbonate formation in oceanic peridotite. Geochim Cosmochim Acta 199:264–286. https://doi.org/10.1016/j.gca.2016.10.052
Hinsken T, Bröcker M, Strauss H, Bulle F (2017) Geochemical, isotopic and geochronological characterization of listvenite from the upper unit on tinos, cyclades, Greece. Lithos 282–283:281–297. https://doi.org/10.1016/j.lithos.2017.02.019
Holland TJB, Powell R (1998) An internally consistent thermodynamic data set for phases of petrological interest. J Metamorph Geol 16:309–343. https://doi.org/10.1111/j.1525-1314.1998.00140.x
Isshiki M, Irifune T, Hirose K et al (2004) Stability of magnesite and its high-pressure form in the lowermost mantle. Nature 427:60–63. https://doi.org/10.1038/nature02181
Johnson JW, Oelkers EH, Helgeson HC (1992) SUPCRT92: a software package for calculating the standard molal thermodynamic properties of minerals, gases, aqueous species, and reactions from 1 to 5000 bar and 0 to 1000°C. Comput Geosci 18:899
Jonas L, Müller T, Dohmen R et al (2015) Transport-controlled hydrothermal replacement of calcite by Mg-carbonates. Geology 43:779–783. https://doi.org/10.1130/G36934.1
Jonas L, Müller T, Dohmen R et al (2017) Hydrothermal replacement of biogenic and abiogenic aragonite by Mg-carbonates—relation between textural control on effective element fluxes and resulting carbonate phase. Geochim Cosmochim Acta 196:289–306. https://doi.org/10.1016/j.gca.2016.09.034
Kelemen PB, Hirth G (2012) Reaction-driven cracking during retrograde metamorphism: Olivine hydration and carbonation. Earth Planet Sci Lett 345–348:81–89. https://doi.org/10.1016/j.epsl.2012.06.018
Kelemen PB, Manning CE (2015) Reevaluating carbon fluxes in subduction zones, what goes down, mostly comes up. Proc Natl Acad Sci USA 112:E3997–E4006. https://doi.org/10.1073/pnas.1507889112
Kelemen PB, Matter J (2008) In situ carbonation of peridotite for CO2 storage. Proc Natl Acad Sci USA 105:17295–17300. https://doi.org/10.1073/pnas.0805794105
Kelemen PB, Matter J, Streit EE et al (2011) Rates and mechanisms of mineral carbonation in peridotite: natural processes and recipes for enhanced, in situ CO2 capture and storage. Annu Rev Earth Planet Sci 39:545–576. https://doi.org/10.1146/annurev-earth-092010-152509
Kelemen PB, Aines R, Bennett E et al (2018) In situ carbon mineralization in ultramafic rocks: natural processes and possible engineered methods. Energy Procedia 146:92–102. https://doi.org/10.1016/j.egypro.2018.07.013
Kerrick DM, Connelly JAD (2001) Metamorphic devolatilization of subducted marine sediments and the transport of volatiles into the Earth's mantle. Nature 411:293–296. https://doi.org/10.1038/35077056
Kimball KL (1990) Effects of hydrothermal alteration on the compositions of chromian spinels. Contrib Miner Petrol 105:337–346. https://doi.org/10.1007/BF00306543
Klein F, Garrido CJ (2011) Thermodynamic constraints on mineral carbonation of serpentinized peridotite. Lithos 126:147–160. https://doi.org/10.1016/j.lithos.2011.07.020
Lafay R, Baumgartner LP, Stephane S et al (2017) Petrologic and stable isotopic studies of a fossil hydrothermal system in ultramafic environment (Chenaillet ophicalcites, Western Alps, France): processes of carbonate cementation. Lithos 294–295:319–338. https://doi.org/10.1016/j.lithos.2017.10.006
Lynne BY, Campbell KA, Moore JN, Browne PRL (2005) Diagenesis of 1900-year-old siliceous sinter (opal-A to quartz) at Opal Mound, Roosevelt Hot Springs, Utah, USA. Sediment Geol 179:249–278. https://doi.org/10.1016/j.sedgeo.2005.05.012
Menzel MD, Garrido CJ, López Sánchez-Vizcaíno V et al (2018) Carbonation of mantle peridotite by CO2-rich fluids: the formation of listvenites in the advocate ophiolite complex (Newfoundland, Canada). Lithos 323:238–261. https://doi.org/10.1016/j.lithos.2018.06.001
Menzel MD, Urai JL, Ukar E et al (2022) Progressive veining during peridotite carbonation: insights from listvenites in Hole BT1B, Samail ophiolite (Oman). Solid Earth 13:1191–1218. https://doi.org/10.5194/se-13-1191-2022
Morohashi K, Okamoto A, Satish-Kumar M, Tsuchiya N (2008) Variations in stable isotope compositions (δ13C, δ18O) of calcite within exhumation-related veins from the Sanbagawa metamorphic belt. J Mineral Petrol Sci 103:361–364. https://doi.org/10.2465/jmps.080620b
Okamoto A, Oyanagi R, Yoshida K et al (2021) Rupture of wet mantle wedge by self-promoting carbonation. Commun Earth Environ 2:1–10. https://doi.org/10.1038/s43247-021-00224-5
Oyanagi R, Okamoto A, Satish-Kumar M et al (2021) Hadal aragonite records venting of stagnant paleoseawater in the hydrated forearc mantle. Commun Earth Environ 2:1–10. https://doi.org/10.1038/s43247-021-00317-1
Phillips GN, Evans KA (2004) Role of CO2 in the formation of gold deposits. Nature 429:860–863. https://doi.org/10.1038/nature02644
Picazo S, Malvoisin B, Baumgartner L, Bouvier AS (2020) Low temperature serpentinite replacement by carbonates during seawater influx in the Newfoundland margin. Minerals. https://doi.org/10.3390/min10020184
Putnis A (2009) Mineral replacement reactions. Rev Mineral. Geochemistry 70:87–124. https://doi.org/10.2138/rmg.2009.70.3
Reed MH (1982) Calculation of multicomponent chemical equilibria and reaction processes in systems involving minerals, gases and an aqueous phase. Geochim Cosmochim Acta 46:513–528. https://doi.org/10.1016/0016-7037(82)90155-7

Ruiz-Agudo E, Putnis CV, Rodriguez-Navarro C, Putnis A (2011) Effect of pH on calcite growth at constant aCa2+/aCO32- ratio and supersaturation. Geochim Cosmochim Acta 75:284–296. https://doi.org/10.1016/j.gca.2010.09.034

Streit E, Kelemen P, Eiler J (2012) Coexisting serpentine and quartz from carbonate-bearing serpentinized peridotite in the Samail Ophiolite, Oman. Contrib Miner Petrol 164:821–837. https://doi.org/10.1007/s00410-012-0775-z

Tamura A, Arai S (2006) Harzburgite–dunite–orthopyroxenite suite as a record of suprasubduction zone setting for the Oman ophiolite mantle. Lithos 90:43–56. https://doi.org/10.1016/j.lithos.2005.12.012

Ulrich M, Muñoz M, Guillot S et al (2014) Dissolution-precipitation processes governing the carbonation and silicification of the serpentinite sole of the New Caledonia ophiolite. Contrib Miner Petrol 167:1–19. https://doi.org/10.1007/s00410-013-0952-8

Wada H, Suzuki K (1982) Carbon isotopic thermometry calibrated by dolomite-calcite solvus temperatures. Geochim Cosmochim Acta 47:697–706

Wang J, Watanabe N, Okamoto A et al (2019) Acceleration of hydrogen production during water-olivine-CO2 reactions via high-temperature-facilitated Fe(II) release. Int J Hydrog Energy 44:11514–11524. https://doi.org/10.1016/j.ijhydene.2019.03.119

Weber J, Cheshire MC, Bleuel M et al (2021) Influence of microstructure on replacement and porosity generation during experimental dolomitization of limestones. Geochim Cosmochim Acta 303:137–158. https://doi.org/10.1016/j.gca.2021.03.029

Zhu M, Baatar M, Miao L et al (2014) Zircon ages and geochemical compositions of the Manlay ophiolite and coeval island arc: implications for the tectonic evolution of South Mongolia. J Asian Earth Sci 96:108–122. https://doi.org/10.1016/j.jseaes.2014.09.004